Taller Divulgativo en el CENIM

28 Enero 2014. 12:30 h
Sala de Conferencias

María M. Aranda y Carlos Capdevila

Herramientas termodinámicas para el diseño de aleaciones metálicas. Modelización de diagramas de fase y su aplicación en el diseño de materiales metálicos

CENIM
Centro Nacional de Investigaciones Metalúrgicas
CSIC
Consejo Superior de Investigaciones Científicas
Vicedirección de Comunicación y Formación. conforma@cenim.csic.es

PARTE I

Principios para el diseño de aleaciones metálicas por medio de herramientas termodinámicas

Termodinámica y Diseño de Materiales

Mecanismo del botijo

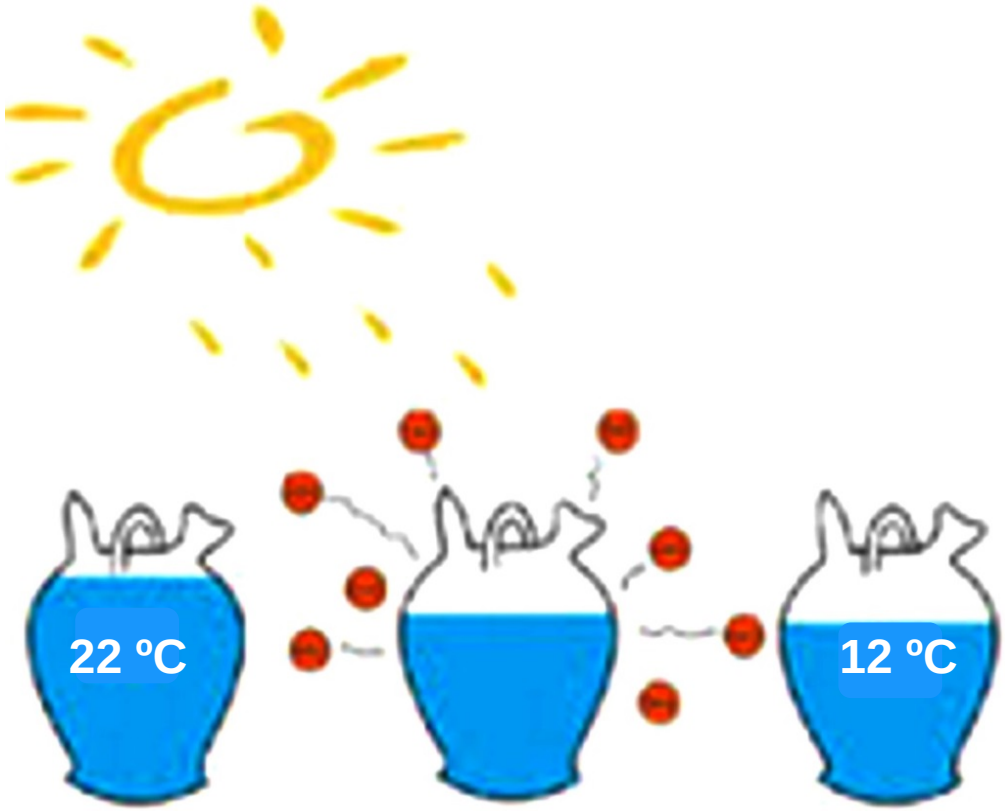

- Selección de materiales en función de su aplicación
- Comportamiento durante la síntesis y el conformado
- Prever y analizar el comportamiento en condiciones de trabajo

Termodinámica y Diseño de Materiales

Mecanismo del botijo

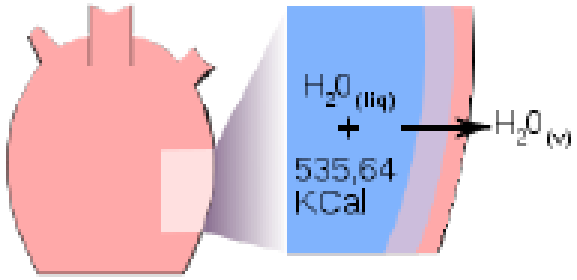

- En 1995, Gabriel Pinto y José Ignacio Zubizarreta de la Universidad Politécnica de Madrid desarrollaron un modelo matemático para un botijo esférico.

$$-\frac{dV}{dt} = K' \cdot a(H_s - H)$$

$$V \cdot C_p \cdot \left(\frac{dT}{dt}\right) = h_c \cdot a \cdot (T_g - T_s) + f \cdot \epsilon \cdot \sigma \cdot (4\pi r^2 - s) \cdot [(273+T_g)^4 - (273+T_s)^4] - U \cdot a \cdot (T - T_s) - \lambda_\omega \cdot \left(\frac{dV}{dt}\right)$$

donde:

V	= volumen del agua
t	= tiempo
C_p	= capacidad calorífica del agua
T	= temperatura del agua
T_g	= temperatura del aire
T_s	= temperatura de la superficie del agua
a	= área de la superficie externa del agua
$4\pi r^2$	= área de la superficie total del botijo
s	= área del agua en contacto con el aire
λ_ω	= calor de vaporización del agua
h_c	= coeficiente de convección
$f \cdot \epsilon \cdot \sigma$	= coeficiente de radiación de calor
U	= coeficiente de transmisión de calor del agua
K'	= coeficiente de transferencia de masa para el agua
H_s	= humedad de saturación
H	= humedad del aire

Gabriel Pinto; José Ignacio Zubizarreta. «Enfriamiento del agua contenida en un botijo». Consultado en wikipedia

Termodinámica y Diseño de Materiales

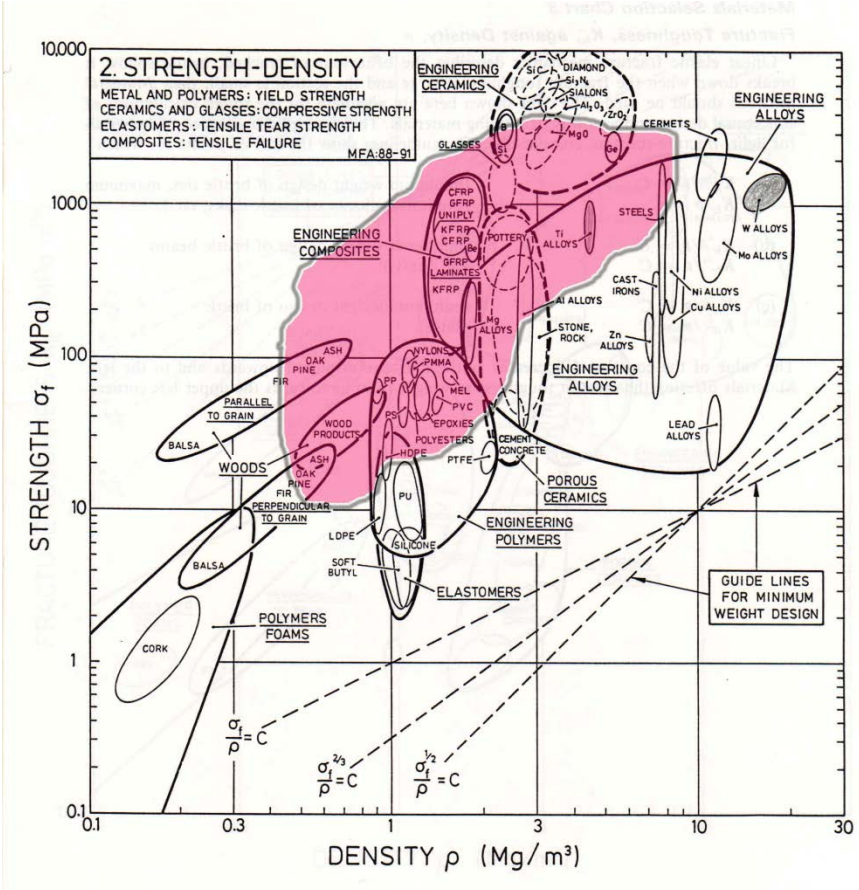

Michael Ashby, Materials Selection in Mechanical Design, 4th Edition, BH (2010)

- Los mapas de propiedades representan los distintos materiales en función de las propiedades que queramos buscar
- En una misma "familia", como los metales, hay una gran variabilidad como consecuencia de la microestructura y de la presencia de distintas fases
- Necesitamos controlar las fases presentes en nuestra aleación, y lo hacemos mediante diagrama fases

Diagrama de equilibrio de fases

- Representación de la combinación de fases estables en un sistema en función de T, P, E, X y P_{gas}

Diagramas de Fase y Materiales Reales

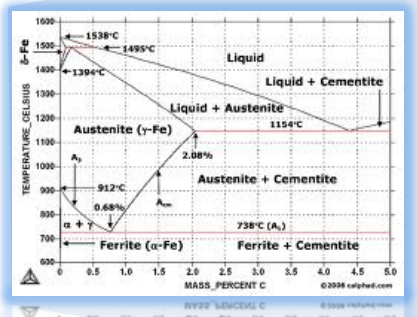

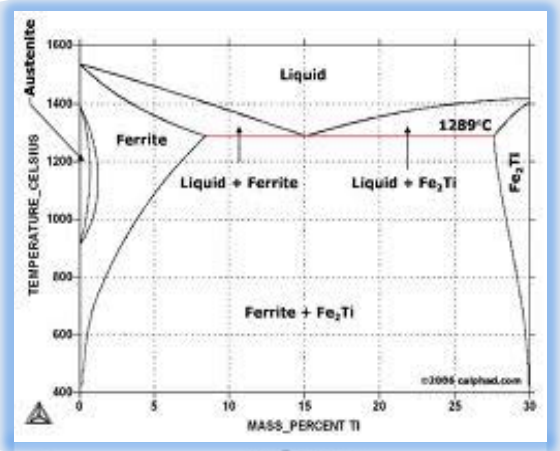

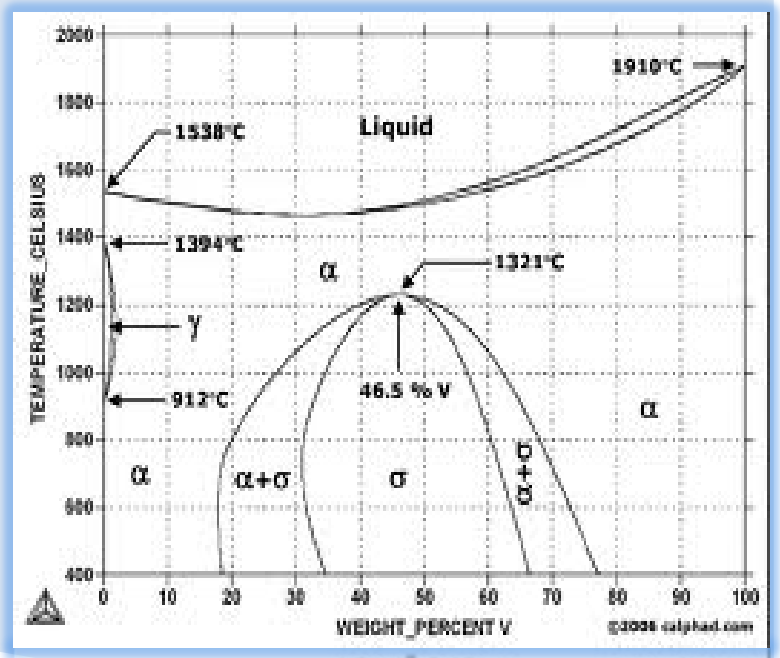

- En los últimos 150 años se han ido acumulando datos experimentales que nos permiten tener una vasta colección de diagramas binarios y ternarios, que son las “fichas” para determinar condiciones de procesado (temperatura y presión) para obtener una determinada microestructura

Diagramas de Fase y Materiales Reales

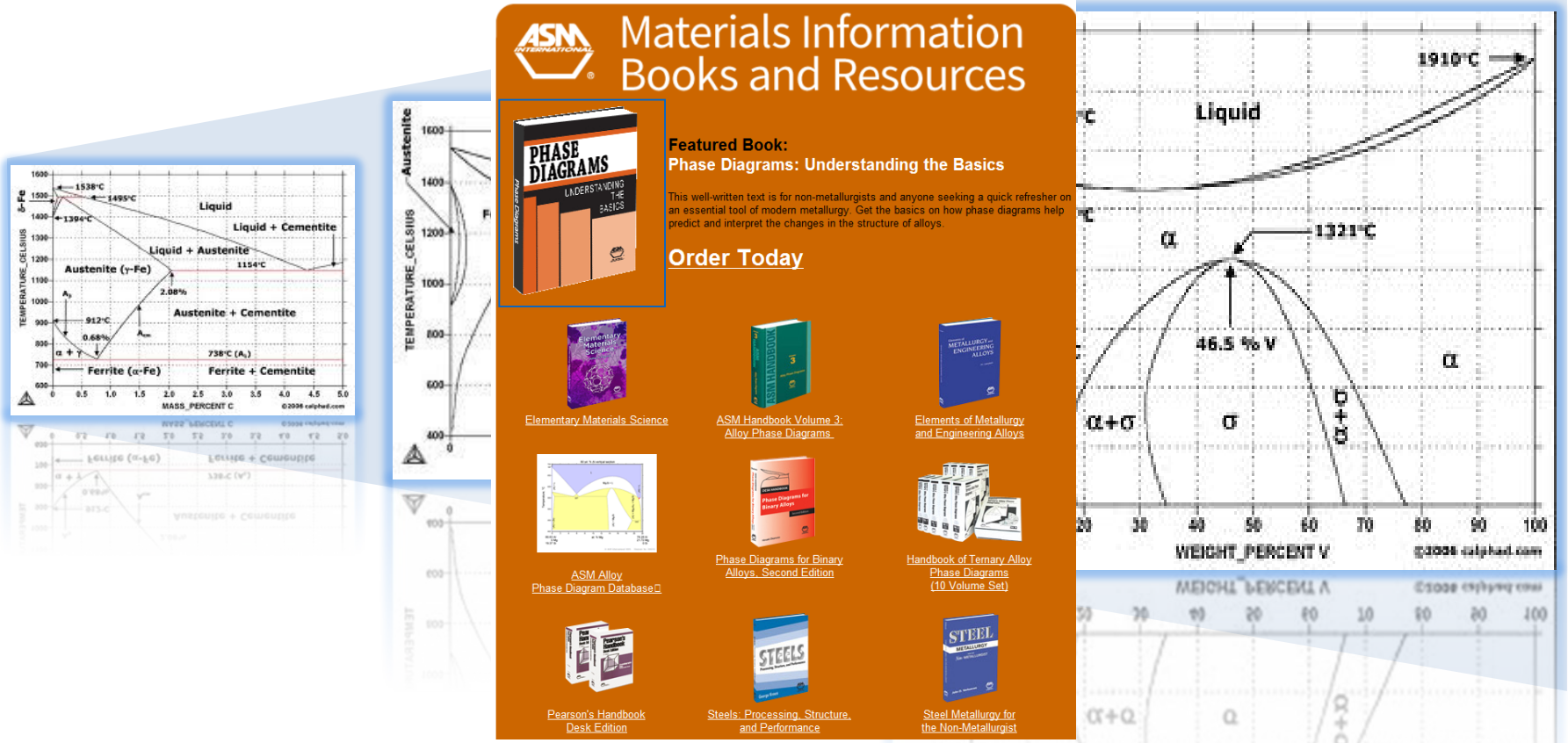

- En los últimos 150 años se han ido acumulando datos experimentales que nos permiten tener una vasta colección de diagramas binarios y ternarios, que son las “fichas” para determinar condiciones de procesado (temperatura y presión) para obtener una determinada microestructura

Diagramas de Fase y Materiales Reales

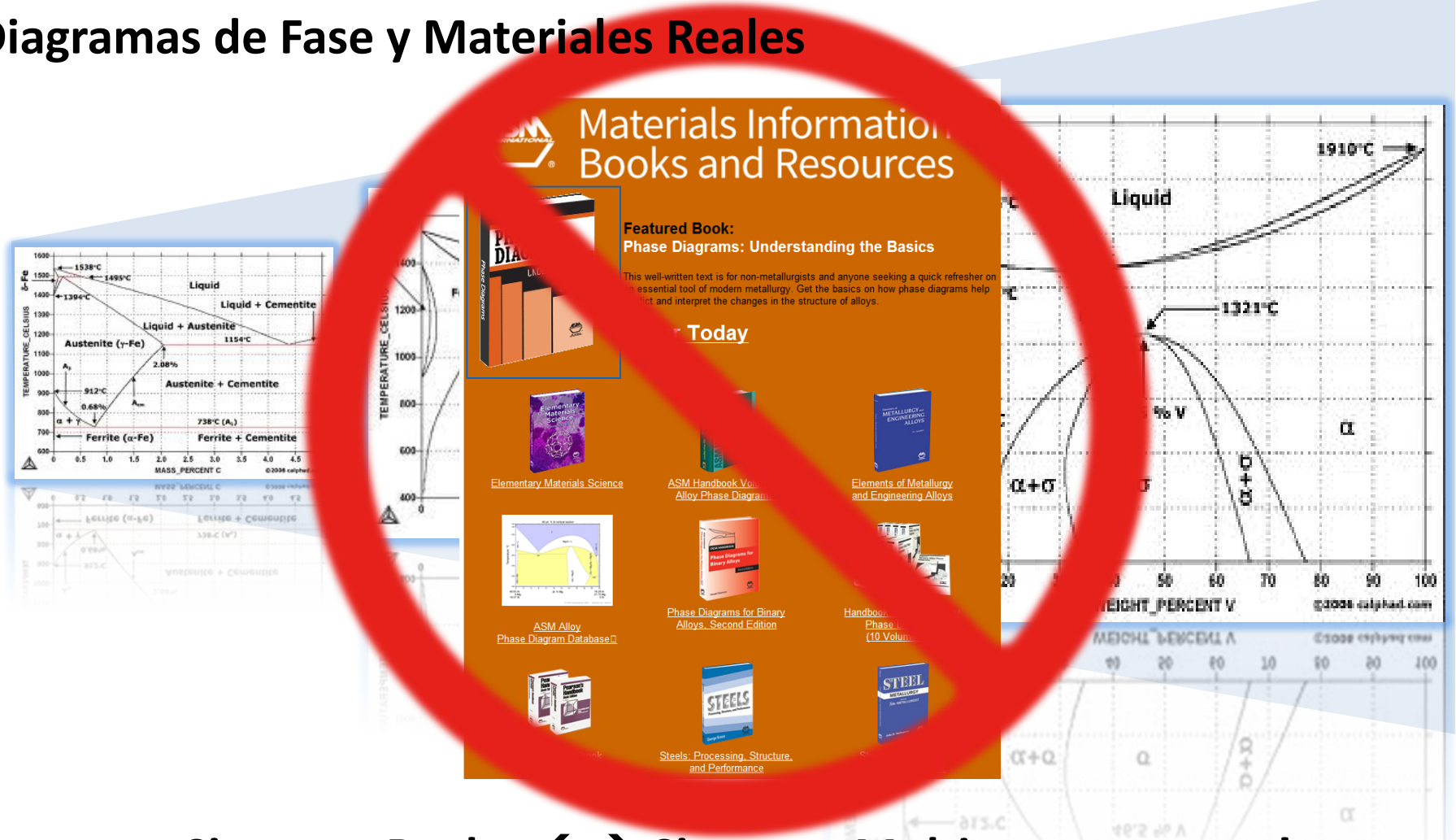

¡ Sistemas Reales ←→ Sistemas Multicomponentes !

- Para estudiar este problema, hace 40 años se pusieron las bases por parte de Larry Kaufman and Himo Ansara de la metodologia CALPHAD (**CAL**culation of **PHA**se **D**iagrams)

Breve reseña del método CALPHAD

- El los 70s científicos de ManLabs (USA); KIT (Suecia); Universidad de Grenoble (Francia) y NPL (Reino unido) aplicaron el concepto de “lattice stabilities” para calcular ΔG entre los distintos estados estables y metaestables de Una fase como función de la temperatura, lo que permitía calcular de forma más precisa las fronteras de equilibrio entre las distintas fases de un sistema

- En 1979, los trabajos de CALPHAD cristalizaron en una base de datos denominada SGTE (Scientific Group Thermodata Europe), que contenía los datos experimentales recopilados hasta el momento para cientos de compuestos inorgánicos y aleaciones, y que por primera vez eran accesibles para toda la Comunidad Europea por medio del sistema de comunicaciones EURONET

- La base de datos SGTE es la matriz de todos las bases de datos posteriores implementadoas dentro de los distintos softwares comerciales que trabajan con este método.

http://www.calphad.org/

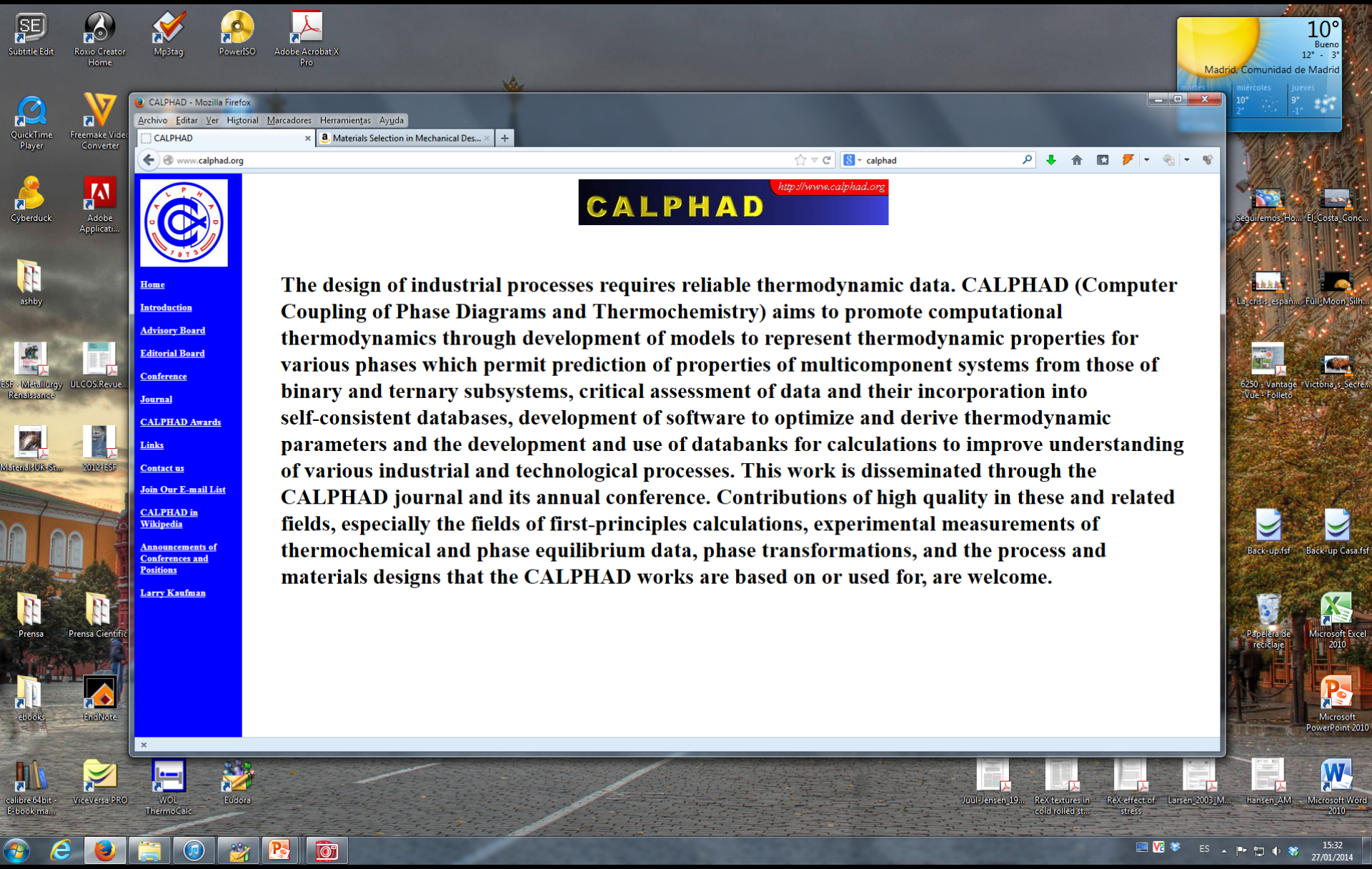

¿En que consiste el método CALPHAD?

DIAGRAMA DE FASES: Representación gráfica de la situación de equilibrio de un sistema

EQUILIBRIO: Configuración de fases que hace mínima la energía libre de Gibbs (G) del sistema

El cálculo de diagramas de equilibrio de fases se basa en el cálculo de G de las fases del sistema

¿En que consiste el método CALPHAD?

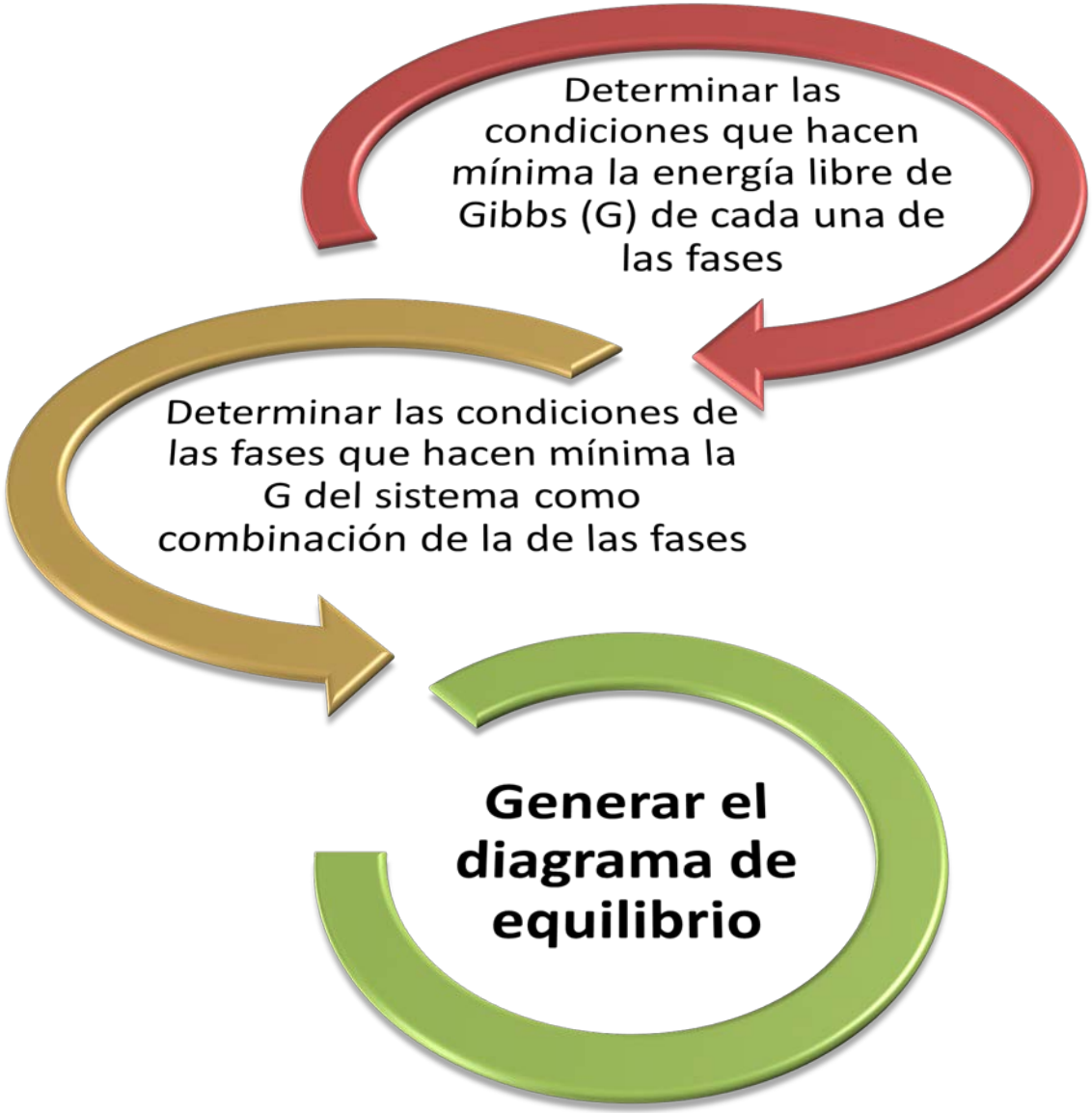

Determinación de una expresión para G

- Encontrar una expresión matemática que describa G en función de las propiedades fisico-químicas de la fase

Sistemas sencillos → sustitución aleatoria

Modelo de Bragg-Williams ➡

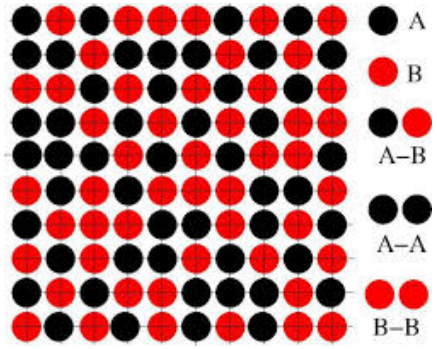

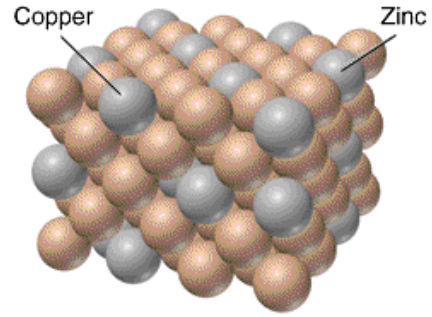

A Brass, a substitutional alloy

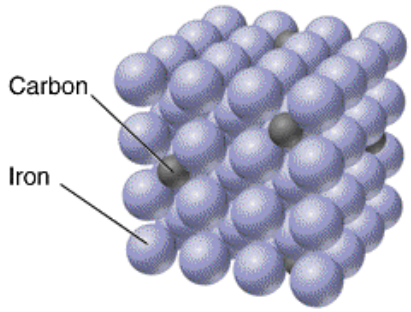

B Carbon steel, an interstitial alloy

Sistemas complejos → modelo sub-redes

Vista de la estructura de Mo_3Sb_7

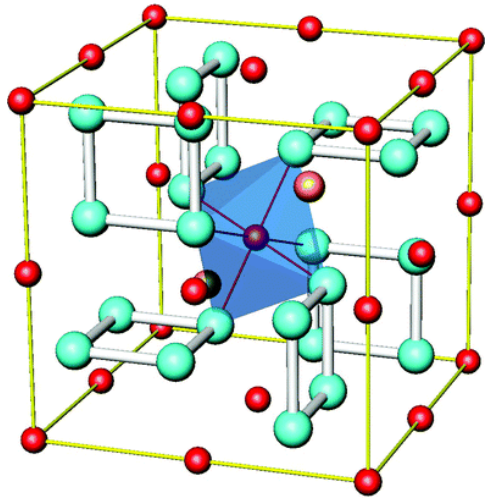

Mo

Sb

Determinación de una expresión para G

$$\Delta G_{sistema} = \sum_{i=2}^{n} x_i \Delta G^0_i + \Delta G_{mezcla}$$

$$\Delta G_{mezcla} = \Delta H_{mezcla} - T\,\Delta S_{mezcla}$$

Sistemas ideales → $\Delta H_{mezcla} = 0$

Sistemas reales → $\Delta H_{mezcla} \neq 0$

Determinación de una expresión para G

Por ejemplo, de forma mas particular para un sistema bifasico, la expresion de G:

$$G = x_A G_A + x_B G_B + \Delta G_{mix}$$

$$\Delta G_{mix} = \Delta H_{mix} - T\Delta S_{mix} = \Delta H_{mix} + RT(x_A \ln x_A + x_B \ln x_B)$$

Soluciones ideales:

$\Delta H_{mix} = 0$ (energía interna del sistema antes y después de la mezcla)

$$G = x_A G_A + x_B G_B + RT(x_A \ln x_A + x_B \ln x_B)$$

Soluciones reales:

$\Delta H_{mix} \neq 0$ (en sistemas reales hay calor absorbido o generado durante la mezcla)

$$G = x_A G_A + x_B G_B + \Omega\, x_A x_B + RT(x_A \ln x_A + x_B \ln x_B)$$

Modelo **cuasi-químico** o de soluciones regulares, donde la entalpia es debido a la energía de enlace entre los átomos vecinos que constituyen una fase

Determinación de una expresión para G

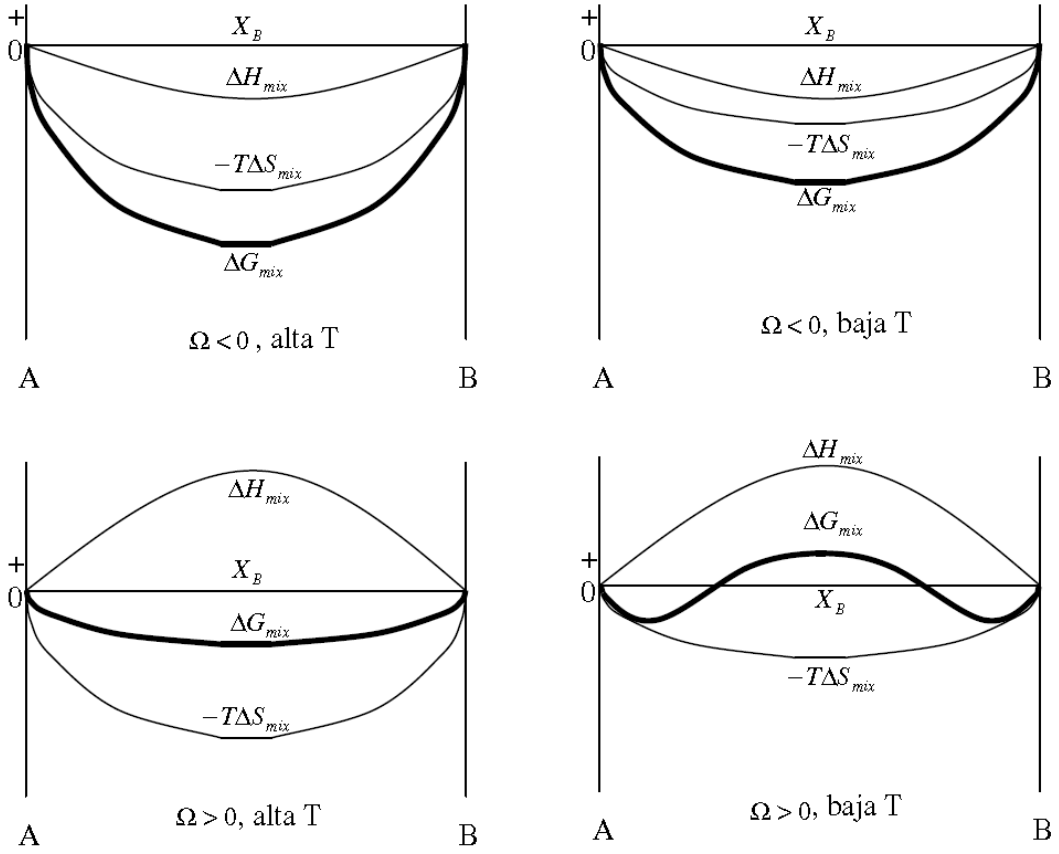

Determinación de una expresión para G

¿Cómo evaluamos la composición química de los elementos que forman una fase?

Potencial químico de A $\mu_A = \left(\frac{\partial G}{\partial n_A}\right)_{T,P,n_B}$

Variación de la *G* al añadir una cantidad *n* del elemento *A* a la fase

G (molar)= $\mu_A x_A + \mu_B x_B$

$$\mu_A = G_A + RTlnx_A$$

$$\mu_B = G_B + RTlnx_B$$

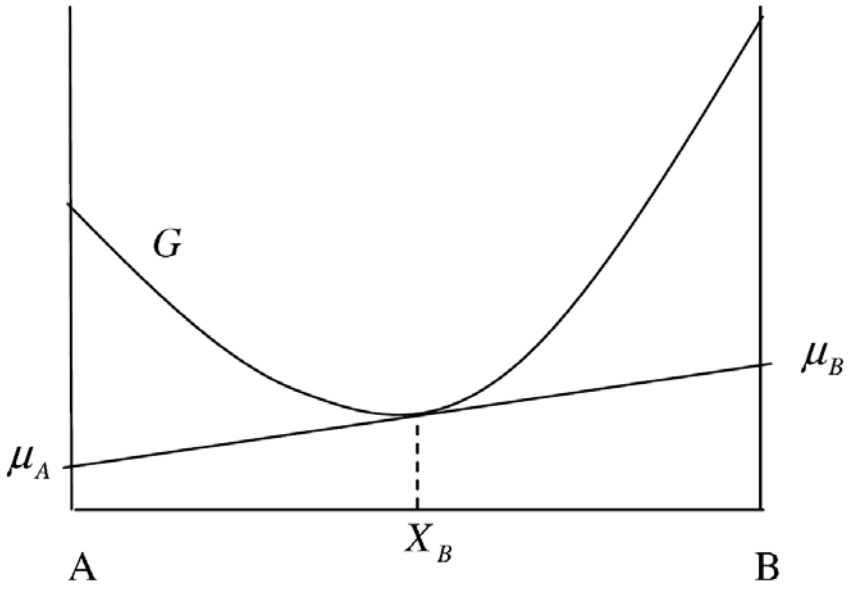

Determinación de una expresión para G

¿Cómo evaluamos la composición química de los elementos que forman una fase?

Actividad de A $\mu_A = G_A + RTlna_A$

Diferencia entre el valor de *G* y el del μ del elemento *A* en la fase

$$\mu_A = G_A + RTlna_A$$

$$\mu_B = G_B + RTlna_B$$

Soluciones reales:

$$ln\left(\frac{a_A}{x_A}\right) = \frac{\Omega}{RT}(1 - X_A)^2$$

$$ln\left(\frac{a_B}{x_B}\right) = \frac{\Omega}{RT}(1 - X_B)^2$$

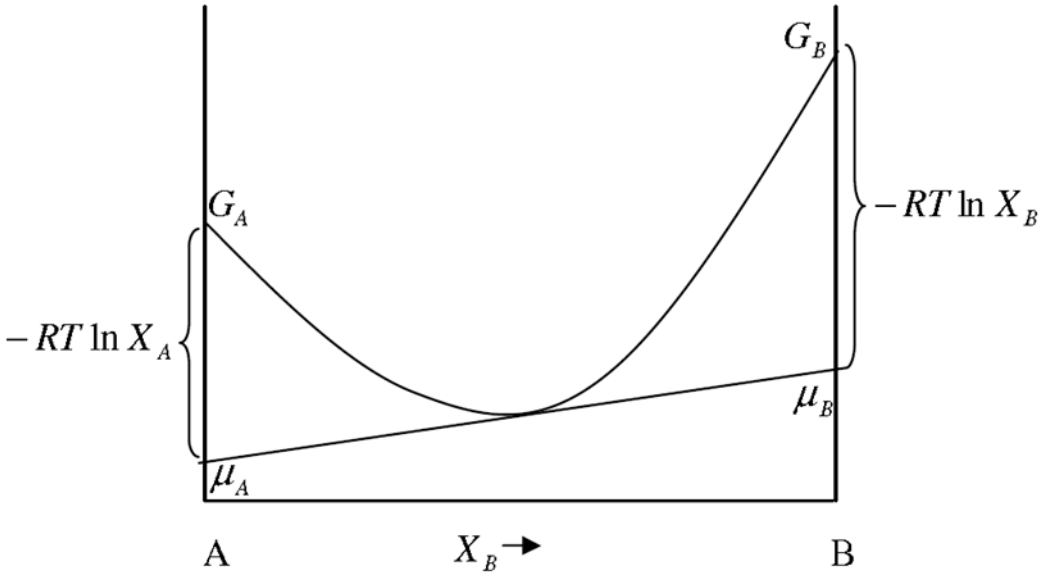

Soluciones ideales, Ω=0 → $a_A = x_A$; $a_B = x_B$

Determinación de una expresión para G

- A medida que suponemos mas interacciones entre los componentes, vamos considerando modelos mas complejos. Así, de soluciones regulares pasamos al modelo que se usa en CALPHAD mas habitualmente que es el sub-regular.

Solución ideal:

$$\Delta G_{mezcla} = 0$$

Solución regular:

$$\Delta G_{mezcla} = x_A \cdot x_B \cdot \left[L_{A-B}^{0,0,1} + L_{A-B}^{0,1,f} \cdot T \right]$$

Solución sub – regular:

$$\Delta G_{mezcla} = x_A \cdot x_B \cdot \left[L_{A-B}^{0,0,1} + L_{A-B}^{0,1,f} \cdot T + (L_{A-B}^{1,0,1} + L_{A-B}^{1,1,f}) \cdot (x_A - x_B) \right]$$

Sol. Diluidas > Sol. Ideales > Sol. Regulares > Sol. sub-Regulares

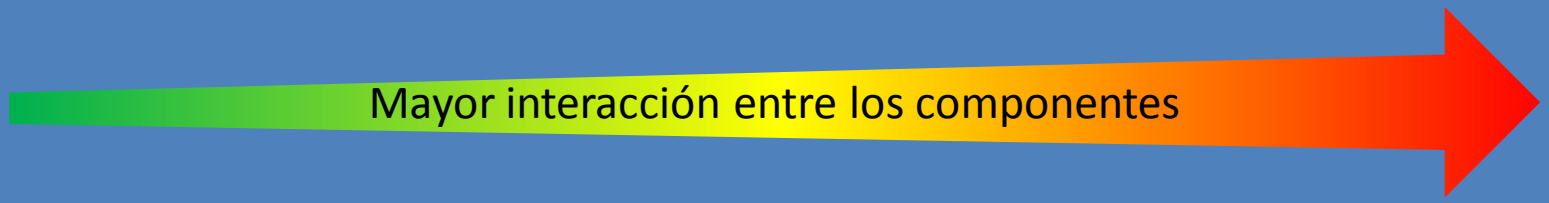

Creación de una BBDD consistente

- Ajustar una expresión de $\Delta G_{sistema}$ bajo un modelo de soluciones sub-regulares a los datos experimentales para poder determinar los coeficientes que son desconocidos

- Una vez hecho esto, ya podemos describir matemáticamente nuestro sistema

- Conseguimos una base de datos consistente

- ¿Y eso qué es?

    1. Pues que tenemos todos los datos en el mismo rango de Temperatura, Presión y composición de validez definido
    2. Descripción continua en especies para el rango de composición definido

Software comercial

- Suites comerciales compuestas de una interface y bases de datos:

Compiten en:

- Dimensión de la base de datos y numero de sistemas incluidos
- El método de ajuste de la función G a los valores experimentales
- Modelos que se usan para describir las fases

Software comercial

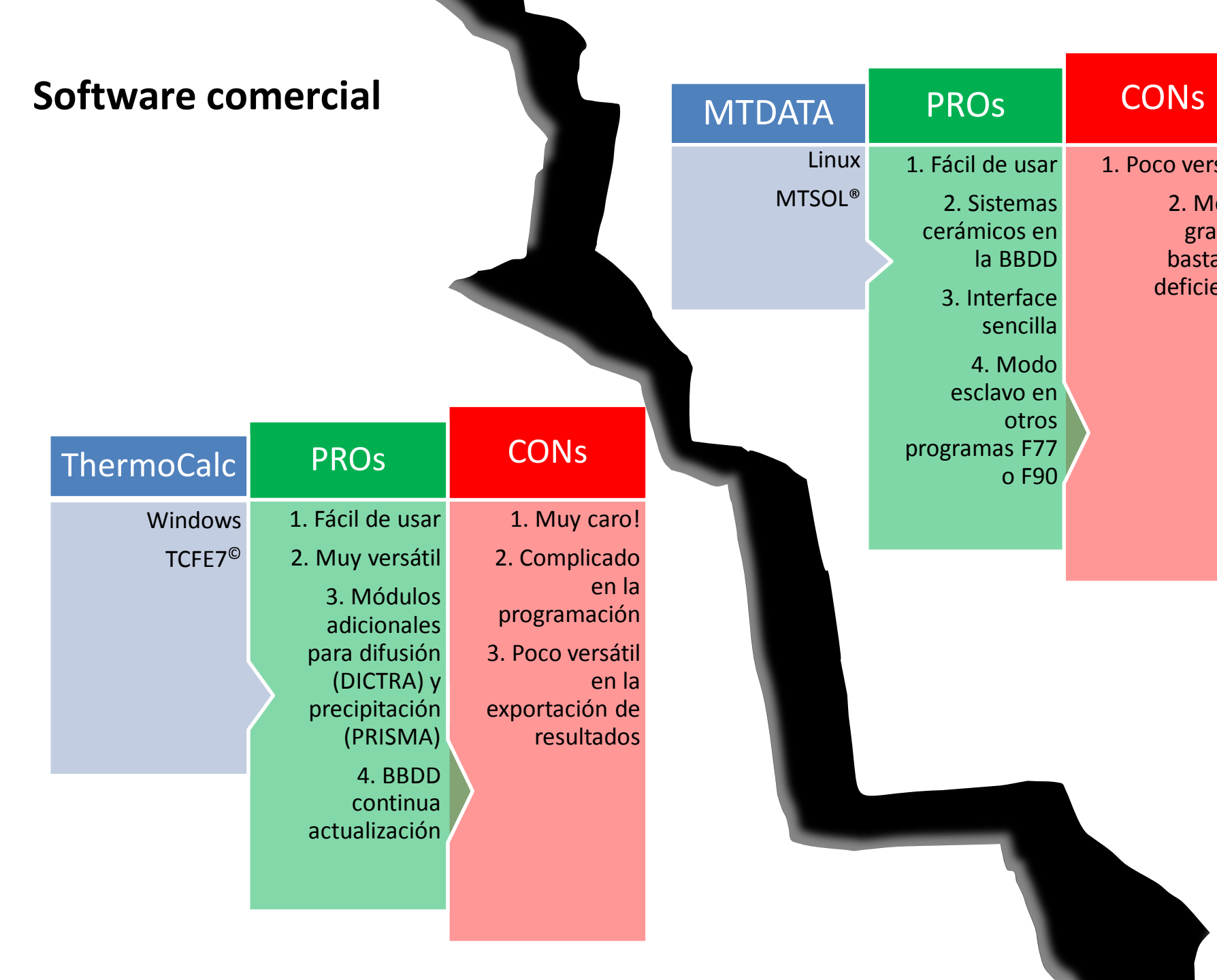

MTDATA	PROs	CONs
Linux MTSOL®	1. Fácil de usar 2. Sistemas cerámicos en la BBDD 3. Interface sencilla 4. Modo esclavo en otros programas F77 o F90	1. Poco versátil 2. Modo grafico bastante deficiente

ThermoCalc	PROs	CONs
Windows TCFE7©	1. Fácil de usar 2. Muy versátil 3. Módulos adicionales para difusión (DICTRA) y precipitación (PRISMA) 4. BBDD continua actualización	1. Muy caro! 2. Complicado en la programación 3. Poco versátil en la exportación de resultados

Ejemplos

Determinación temperatura Ms en Fe-0.4C-x_1Co-x_2Cr

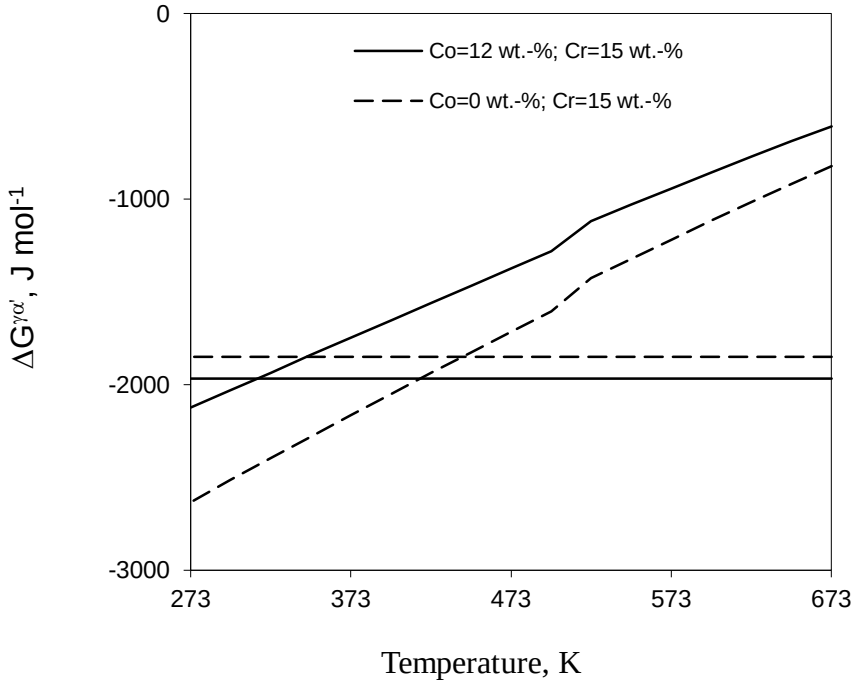

ISIJ International, Vol. 42 (2002), No. 8, pp. 894–902

Determination of Ms Temperature in Steels: A Bayesian Neural Network Model

C. CAPDEVILA, F. G. CABALLERO and C. GARCÍA DE ANDRÉS

Department of Physical Metallurgy, Centro Nacional de Investigaciones Metalúrgicas (CENIM), CSIC, Avda. Gregorio del Amo, 8, 28040 Madrid, Spain. E-mail: cgda@cenim.csic.es

(*Received on March 15, 2002; accepted in final form on May 13, 2002*)

The knowledge of the martensite start (Ms) temperature of steels is sometimes important during parts and structures fabrication, and it can not be always properly estimated using conventional empirical methods. The additions in newly developed steels of alloying elements not considered in the empirical relationships, or with compositions out of the bounds used to formulate the equations, are common problems to be solved by experimental trial and error. If the trial process was minimised, cost and time might be saved. This work outlines the use of an artificial neural network to model the calculation of Ms temperature in engineering steels from their chemical composition. Moreover, a physical interpretation of the results is presented.

KEY WORDS: neural network analysis; martensite; modelling phase transformation; steels.

1. Introduction

The Ms temperature is of vital importance for engineering steels. Hence great efforts have been made in predicting the Ms temperature of these steels. Obviously, chemical composition of steel is the main factor affecting its Ms although the austenitising state, external stresses and stored deformation energy may sometimes play an important role as well. Martensite start temperatures are usually relatively easy to calculate as long as the steels have a low alloy content.[1–5] Even though empirical equations exists for high alloy steels, they are not sufficiently general and are known to provide inaccurate answers for the new steels which contain different alloying elements, or their compositional range are out of bounds of those used to formulate the equations.

For instance, the interest of copper additions to the chemical composition of steels has increase in the last years. Copper-bearing low carbon steels are used in heavy engineering applications which demand a combinations of strength, toughness and weldability.[7–11] Strength is achieved by precipitation of fine copper precipitates during ageing, instead of precipitation of carbide particles.[8] Therefore, copper is not in this respect different from any secondary hardening element in steels. Likewise, it has been demonstrated that copper sulphide strongly enhance acicular ferrite formation, which induces a good combination of mechanical properties as compared to bainite and especially to ferrite–pearlite microstructures.[12–15]

Likewise, power stations are nowadays designated to operate with steam temperatures in excess of 873 K. The steels currently being developed to cope with these requirements contain a total solute concentration which is often in excess of 14 wt%. The main solutes include carbide forming elements such as chromium and molybdenum. Chromium also provides the necessary corrosion and oxidation resistance for prolonged elevated temperature service. The main alloys under consideration include numerous variants of the classical 12Cr–1Mo and 9Cr–1Mo steels.[16,17] These alloys have a high hardenability and a microstructure which is predominantly martensitic on cooling from the austenitising temperature. Their martensitic start Ms temperature is therefore of considerable importance in deciding on the exact welding conditions necessary to avoid cracking.[17] An important variant of the 9Cr–1Mo steel is that in which tungsten is added to induce precipitation hardening.[18]

Gustafson and Ågren[19] reported that Co has a remarkable influence on coarsening of $M_{23}C_6$ carbides in the 9Cr–1Mo steel. Their results show that a final average radius of the carbides after 30 000 h at 873 K decreases in 30% with a Co addition of 10 mass%. This raises the Orowan stress with 30%. Moreover, it is assumed that slower particle coarsening also leads to a retard in the coarsening of the martensite lath structure. Thus, an improvement on creep life of the steels is expected.[19]

Likewise, it has been reported that the combined additions of cobalt and tungsten to the chemical composition strengthen the steel by precipitation of tungsten–cobalt (WC–Co) cemented carbides.[20] These new steels are widely used as tool steels where a good combination between abrasion resistance and corrosion resistance is required.[21–23]

It is then followed that the investigation of how copper, tungsten, and cobalt additions may affect the Ms temperature is an important issue. Thus, the aim of this work is to

© 2002 ISIJ

Critical value in J mol^{-1} of the driving force needed to trigger martensitic transformation:

$$-\Delta G_C^{\gamma\alpha'} = 683 + 4009c_C^{0.5} + 1879c_{Si}^{0.5} + 1980c_{Mn}^{0.5} + 172c_C^{0.5} + 1418c_{Mo}^{0.5} + 1868c_{Cr}^{0.5}$$
$$+ 1618c_V^{0.5} + 752c_{Cu}^{0.5} + 714c_W^{0.5} + 1653c_{Nb}^{0.5} + 3097c_N^{0.5} - 352c_{Co}^{0.5}$$

Ejemplos

Descomposición spinodal en el sistema Fe-Cr-Al-Ti

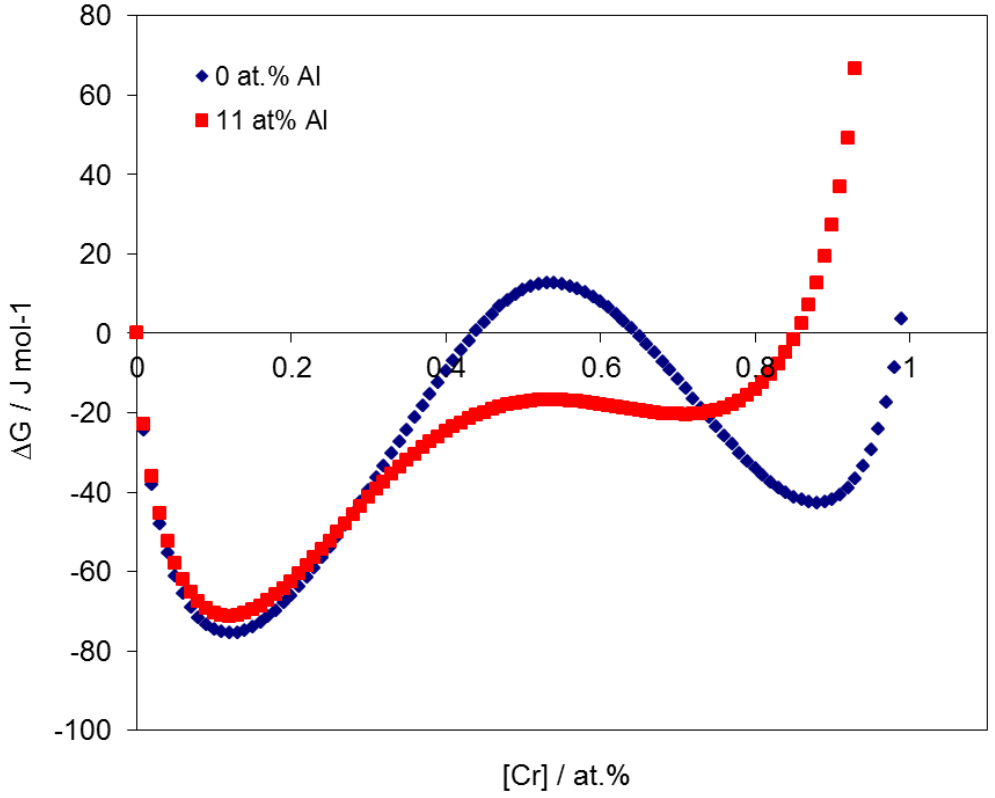

ΔG_{mezcla} en el sistema Fe-Cr-Al-0.5Ti

Available online at www.sciencedirect.com
SciVerse ScienceDirect
Acta Materialia 60 (2012) 4573–4584
Acta MATERIALIA
www.elsevier.com/locate/actamat

Phase separation kinetics in a Fe Cr Al alloy

C. Capdevila [a,*], M.K. Miller [b], J. Chao [a]

[a] Materalia Group, Centro Nacional de Investigaciones Metalúrgicas (CENIM-CSIC), Avenida Gregorio del Amo, 8, 28040 Madrid, Spain
[b] Materials Science and Technology Division, Oak Ridge National Laboratory, PO Box 2008, Oak Ridge, TN 37831-6136, USA

Received 22 March 2012; received in revised form 14 May 2012; accepted 15 May 2012
Available online 26 June 2012

Abstract

The α–α′ phase separation kinetics in a commercial Fe–20 wt.% Cr–6 wt.% Al oxide dispersion-strengthened PM 2000™ steel have been characterized with the complementary techniques atom probe tomography and thermoelectric power measurements during isothermal aging at 673, 708, and 748 K for times up to 3600 h. A progressive decrease in the Al content of the Cr-rich α′ phase was observed at 708 and 748 K with increasing time, but no partitioning was observed at 673 K. The variation in the volume fraction of the α′ phase well inside the coarsening regime, along with the Avrami exponent 1.2 and activation energy 264 kJ mol $^{-1}$, obtained after fitting the experimental results to an Austin–Rickett type equation, indicates that phase separation in PM 2000™ is a transient coarsening process with overlapping nucleation, growth, and coarsening stages.
© 2012 Acta Materialia Inc. Published by Elsevier Ltd. All rights reserved.

Keywords: Phase separation; Ferrous alloy; Mechanical alloying; Tomography; Thermoelectric power

1. Introduction

The Fe Cr Al oxide dispersion-strengthened (ODS) ferritic steels are manufactured by a complex powder metallurgy route. Due to their high creep rupture strength and excellent swelling resistance many ODS ferritic steels are under development for several types of nuclear reactors, such as sodium fast reactors (SFR) or supercritical water reactors (SCWR) [1,2]. In such applications these alloys face severe embrittlement problems because their service temperature is in the range 373 823 K. In this temperature range the response of the materials to extreme conditions (high temperatures and irradiation resulting in swelling and corrosion) is partly determined by the extent of α α′ phase separation. Thus, in the last few years binary Fe Cr model alloys have been the focus of significant basic research [3 8].

In the present study atom probe tomography (APT) and thermoelectric power (TEP) measurements were used to monitor the kinetics of Cr diffusion during the α α′ phase separation process. APT is a unique technique that provides highly accurate quantitative data regarding the evolution of phase composition, size, morphology, and number density in the nm scale range during α α′ phase separation. TEP provides macroscopic volumetric information on the response of a material to aging treatments and is also a powerful method to study the dissolution process of carbides in steels, as this technique is very sensitive to the number of atoms in solid solution in iron [9,10]. Therefore, the combination of TEP and APT was used to determine not only the composition of the phases involved, but also the kinetic parameters needed to characterize α α′ phase separation during aging (isothermal heat treatment) of PM 2000™ ODS alloy.

Isothermal reactions allow a detailed analysis of α′ phase precipitation kinetics from a direct fit of the data to the Johnson Mehl Avrami Kolmogorov (JMAK) [11 13] and Austin Rickett (AR) [14] relations. From these analyses kinetic parameters, such as the so-called Avrami exponent and the activation energy, can be calculated to provide a significant understanding of the nucleation and growth processes of α′ precipitates.

* Corresponding author.
E-mail address: ccm@cenim.csic.es (C. Capdevila).

1359-6454/$36.00 © 2012 Acta Materialia Inc. Published by Elsevier Ltd. All rights reserved.
http://dx.doi.org/10.1016/j.actamat.2012.05.022

Ejemplos

New approach for the bainite start temperature calculation in steels

C. García-Mateo*[1], T. Sourmail[2], F. G. Caballero[1], C. Capdevila[1] and C. García de Andrés[1]

The bainite start temperature B_s is defined as the highest temperature at which ferrite can transform by a displacive transformation. A common observation is that the bainite start temperature is very sensitive to the chemical composition, indicating that the influence of solutes is more than just thermodynamic. Empirical linear regression models have long been used to calculate the B_s in a limited range of compositions. This paper attempts to create an empirical model of wider applicability and higher accuracy by means of neural networks. The results are compared with those calculated using the thermodynamic theory for bainite transformation, revealing that in general this theory agrees with the experimental results, but some discrepancies can still be found when the alloys are heavily alloyed.

Keywords: Bainite start temperature, Neural network, Bayesian framework, Thermodynamics theory

Introduction

Because of its mechanical properties and low cost, bainitic steel is being increasingly used in a number of industrial applications, ranging from rails to formula one gearboxes. The bainitic structure develops at temperatures between that for pearlite formation and the martensite start temperature. The exact value of these temperatures depends strongly on the elements present in the steel, and considerable work has been devoted to developing quantitative models for their compositional dependency. Early approaches for predicting the bainite B_s and the martensite start M_s temperatures essentially consisted of the fitting of simple linear empirical relationships.[1–9] Though easily communicated and interpreted, such methods often have very limited ranges of applicability because of their inability to grasp interactions or nonlinear effects. With the development of calculation frameworks such as CALPHAD, which allow prediction of thermodynamic properties of complex systems from data collected on simpler ones, more physically relevant approaches relying on the satisfaction of some thermodynamic criterion have gained importance.[10,11] These are briefly introduced in the next section. In general, such models extrapolate considerably better than the early empirical approaches. However, they suffer a number of drawbacks:

(i) being essentially self-consistent, these approaches require that identical thermodynamic databases are used in the predictions as those which were used for the derivation of the criteria. With the multiplication of databases (SGTE SSOL, NPL plus, TCFE, Kmart), this is increasingly becoming a problem. Recent work by the authors[12] shows, for example, that the recent improvement[13] on a model developed by Ghosh and Olson[14] for predicting M_s performs significantly worse than the original model if the appropriate database is not used

(ii) such approaches rely on the availability of expensive thermodynamic calculation software, the costs of which are hardly justified for such an application alone

(iii) the empirical component is not eliminated but displaced to lower levels of the model.

New empirical methods such as neural network (NN) analysis offer attractive advantages, being not only easily distributed and self-sufficient but also able to cover arbitrarily large ranges of data. As any other method, their domain of applicability is somewhat determined by the data available at the time the model is defined. However, a feature unique to the method employed in the present work is the ability of the model to accompany its predictions by an indication of their reliability.

Predicting the B_s temperature

In this section a brief description of neural network modelling is presented along with the thermodynamic theory for bainite transformation. The latter is necessary in order to understand the results and to be able to compare them with the empirical predictions obtained by means of the NN model developed in this paper.

[1]Department of Physical Metallurgy, Centro Nacional de Investigaciones Metalúrgicas (CENIM), Consejo Superior de Investigaciones Científicas (CSIC), Avda. Gregorio del Amo, 8, 28040 Madrid, Spain
[2]Department of Materials Science and Metallurgy, University of Cambridge, Pembroke Street, Cambridge CB2 3QZ, UK

*Corresponding author, email cgm@cenim.csic.es

© 2005 Institute of Materials, Minerals and Mining
Published by Maney on behalf of the Institute
Received 19 July 2004; accepted 13 May 2005
DOI 10.1179/174328405X51622

Ejemplos

Available online at www.sciencedirect.com
ScienceDirect
Acta Materialia 61 (2013) 6983–6992
Acta MATERIALIA
www.elsevier.com/locate/actamat

The effect of silicon on the nanoprecipitation of cementite

B. Kim [a], C. Celada [b], D. San Martín [b], T. Sourmail [c], P.E.J. Rivera-Díaz-del-Castillo [a,*]

[a] Department of Materials Science and Metallurgy, University of Cambridge, Pembroke Street, Cambridge CB2 3QZ, UK
[b] MATERALIA Group, Department of Physical Metallurgy, Centro Nacional de Investigaciones Metalúrgicas (CENIM-CSIC), Av. Gregorio del Amo 8, 28040 Madrid, Spain
[c] ASCOmetal-CREAS (Research Centre) Metallurgy, BP 70065 57301 Hagondange Cedex, France

Received 21 June 2013; received in revised form 1 August 2013; accepted 6 August 2013
Available online 5 September 2013

Abstract

The current work presents a comprehensive study that aims at understanding the role of silicon on θ precipitation, as well as on the $\varepsilon \rightarrow \theta$ carbide transition in tempered martensite. Cementite nucleation was modelled under paraequilibrium conditions in order to ensure the presence of silicon in the carbide, where both thermodynamic and misfit strain energies were calculated to evaluate the overall free energy change. The growth stage was investigated using in situ synchrotron radiation; three alloys containing 1.4–2.3 wt.% silicon contents have been studied. Silicon appears to play a significant role in carbide growth. It was observed throughout tempering that cementite precipitation was slower in the higher silicon content alloy. Literature reports that cementite growth is accompanied by silicon partitioning, where the silicon content inside the carbide decreases as tempering progresses. Therefore it appears that the limiting factor of the growth kinetics is the rate at which silicon is rejected from the carbide; the silicon piles up at the carbide-matrix interface, acting as a barrier for further growth.
© 2013 Acta Materialia Inc. Published by Elsevier Ltd. All rights reserved.

Keywords: Phase transformation; Synchrotron radiation; Carbides; Precipitation kinetics; Tempered martensite

1. Introduction

It is a well-established fact that silicon plays a retarding effect on the epsilon to cementite carbide transition in tempered martensitic steels [1,2]. This concept has attracted considerable industrial interest in the optimization of alloying in steels – see e.g. Nam et al. [3]. The retention of the ε carbide phase leads to ultrahigh strength in steels, a property attributed to the presence of microstrains at the precipitate–matrix interface [4]. Consequently, near the $\varepsilon \rightarrow \theta$ transition a softening regime exists, where ductility is recovered at the expense of loss in strength. Being of considerable interest from both the academic and the industrial point of view, the role of silicon during tempering has been studied extensively over the past decades. This project's initial interest was in the development of ultra-high-strength steels applications, where one aim was to understand the effect of silicon on carbide precipitation, which is the main focus of the current paper. By understanding the carbide transition at the microstructural level, alloy tailoring can be achieved, whereby improved mechanical properties allow for greater flexibility in designing structural components.

The general understanding has been that the $\varepsilon \rightarrow \theta$ transition, also known as the third stage of tempering, takes place in two steps: Stage IIIA, where the remaining C atoms within the matrix are taken up for cementite precipitation while ε-carbide persists in the matrix. At Stage IIIB it has been thought that once the matrix becomes depleted, the ε-carbide decomposes in order to assist in the further production of cementite. The kinetics has been related to the diffusion of carbon through low-carbon martensite in Stage IIIA, and to the mobility of substitutional elements or the self-diffusion of iron in Stage IIIB. The

* Corresponding author.
E-mail address: pejr2@cam.ac.uk (P.E.J. Rivera-Díaz-del-Castillo).

1359-6454/$36.00 © 2013 Acta Materialia Inc. Published by Elsevier Ltd. All rights reserved.
http://dx.doi.org/10.1016/j.actamat.2013.08.012

¿Conclusión?

La metodología CALPHAD y los cálculos de primeros principios (Ab-initio) enfocados a determinar los parámetros necesarios para los cálculos de G en nuevos sistemas de aleación constituyen una poderosa herramienta de simulación en ciencia de materiales: **Termodinámica computacional**

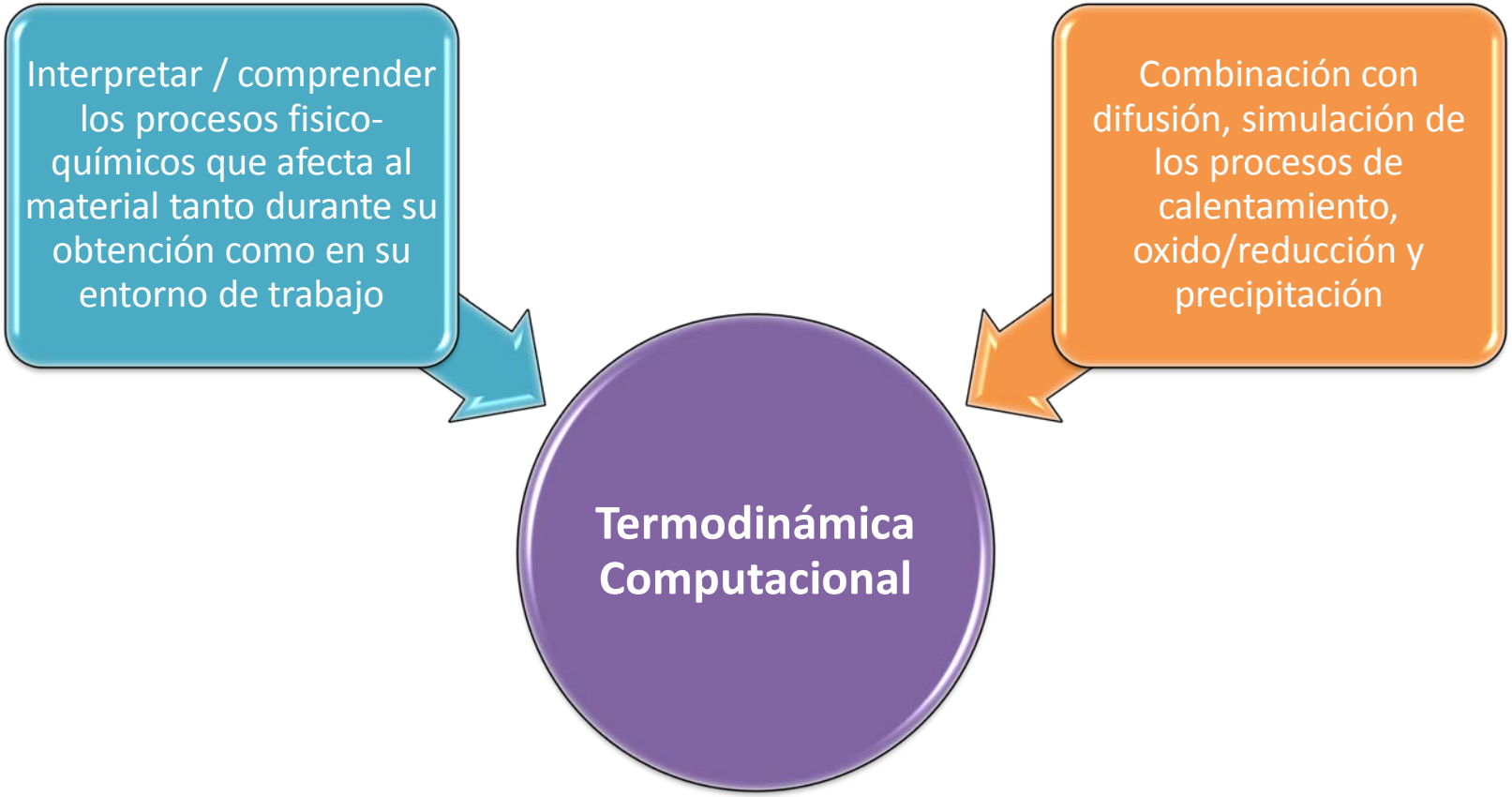

Taller Divulgativo en el CENIM

PARTE II: APLICACIÓN DE THERMOCALC EN LA TRANSFORMACIÓN PERLÍTICA.

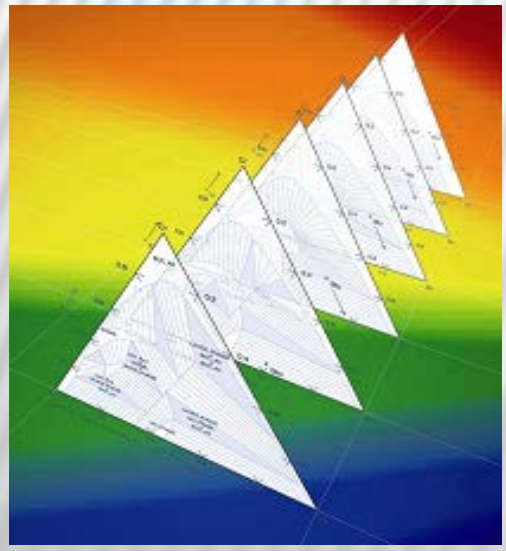

M.M.Aranda
C.Capdevila

Thermo-Calc Software
www.thermocalc.com

ÍNDICE

1.-INTRODUCCIÓN.

2.-CÁLCULO DE DIAGRAMAS DE FASE: ISOPLETH E ISOTHERM.

3.-EXTRAPOLACIÓN DE HULTGREN.

4.-LÍNEAS DE PARTICIÓN-NO PARTICIÓN.

5.- COMPOSICIÓN DE LAS FASES.

1.- INTRODUCCIÓN

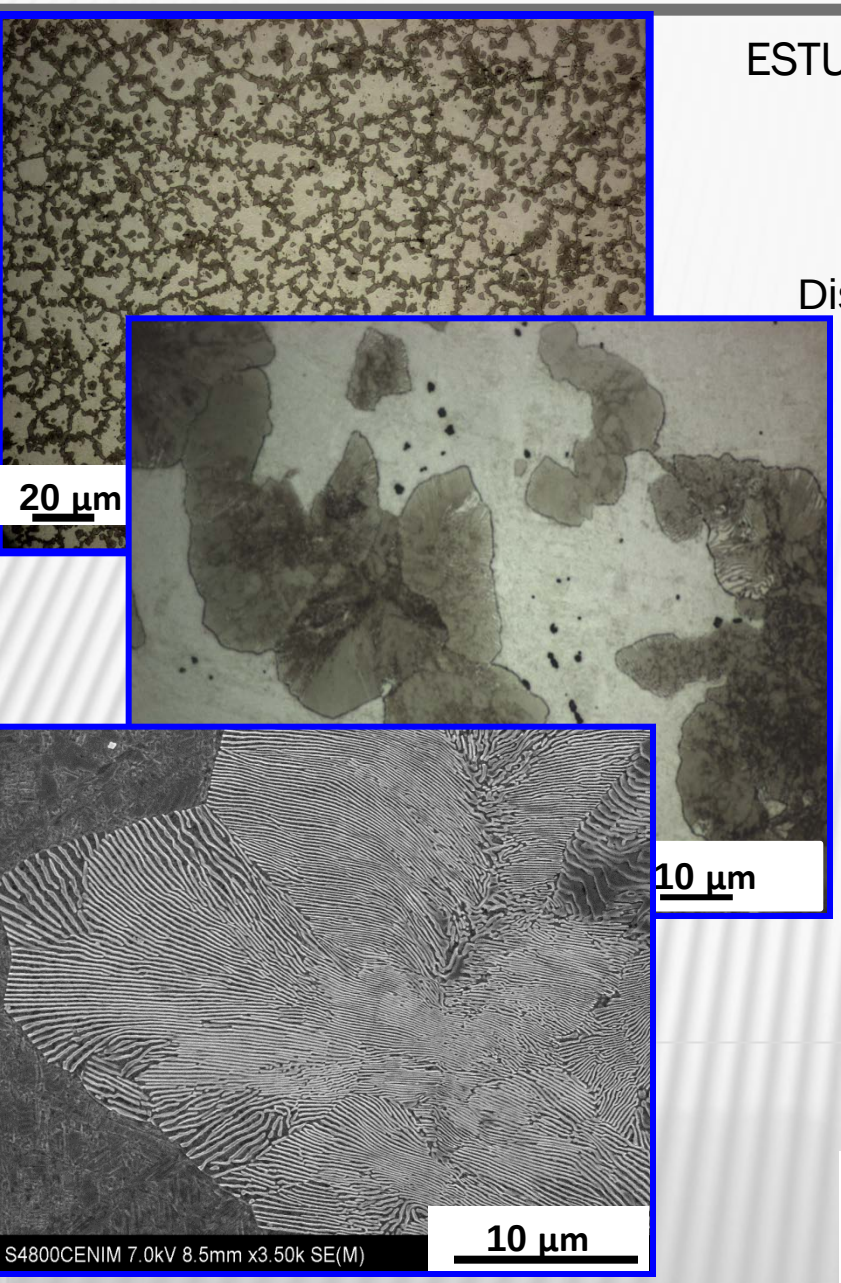

ESTUDIO DE LA TRANSFORMACIÓN PERLÍTCA EN UNA ALEACIÓN Fe-C-Mn.

Diseñar los tratamientos isotérmicos adecuados para el estudio de la transformación perlítica.

- DIAGRAMAS DE FASE.
- EXTRAPOLACIÓN DE HULGTREN.
- ELCP O ELSP: Localización de las regiones de Partición-no partición.
- COMOPOSICIONES INTERCARAS, COMPOSICIONES EQUILIBRIO.
- PERLITA CONSTANTE Y PERLITA DIVERGENTE

Thermo-Calc Software
www.thermocalc.com

CÁLCULO DE DIAGRAMAS DE FASE: ISOPLETH E ISOTHERM

ISOPLETH

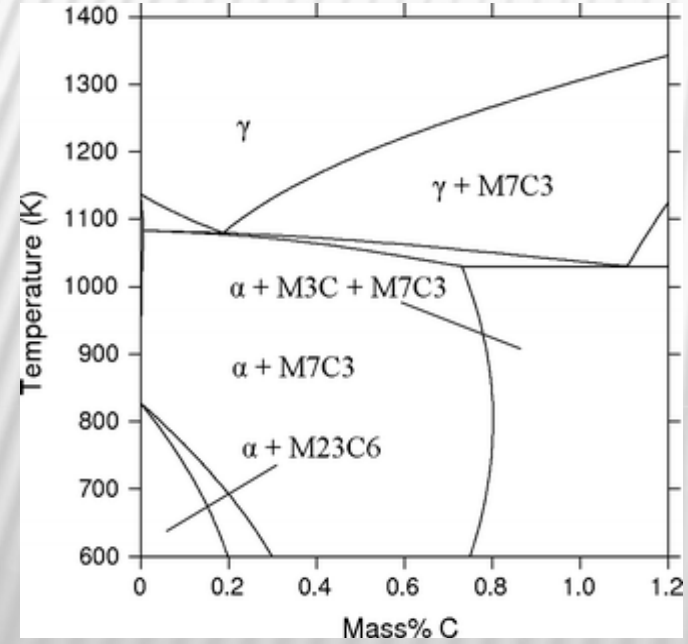

ISOTHERM

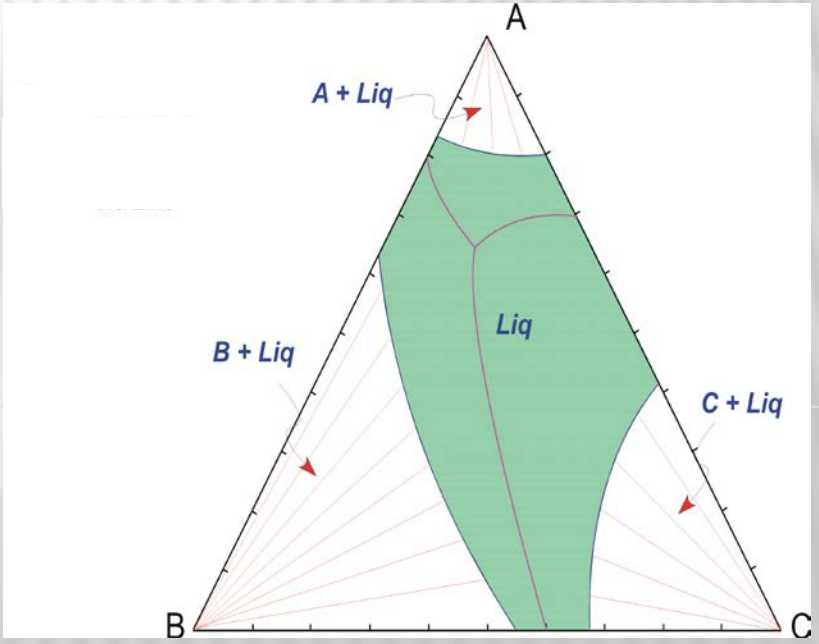

2.- CÁLCULO DE DIAGRAMAS DE FASE: ISOPLETH E ISOTHERM

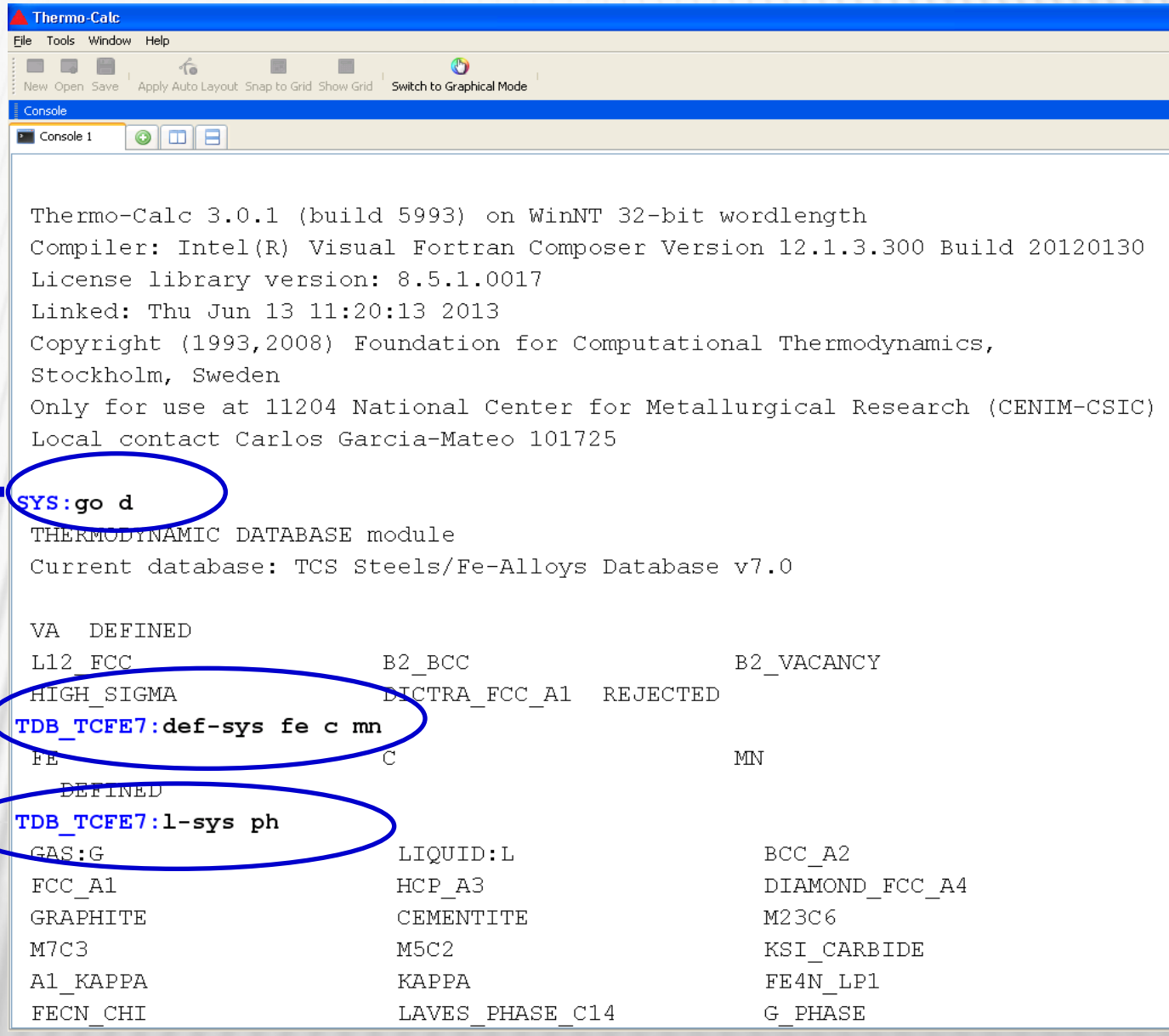

Seleccionar la base de datos

Definir la aleación

Posibles Fases

2.- CÁLCULO DE DIAGRAMAS DE FASE: ISOPLETH E ISOTHERM

Seleccionar las posibles fases presentes para la aleación de interés

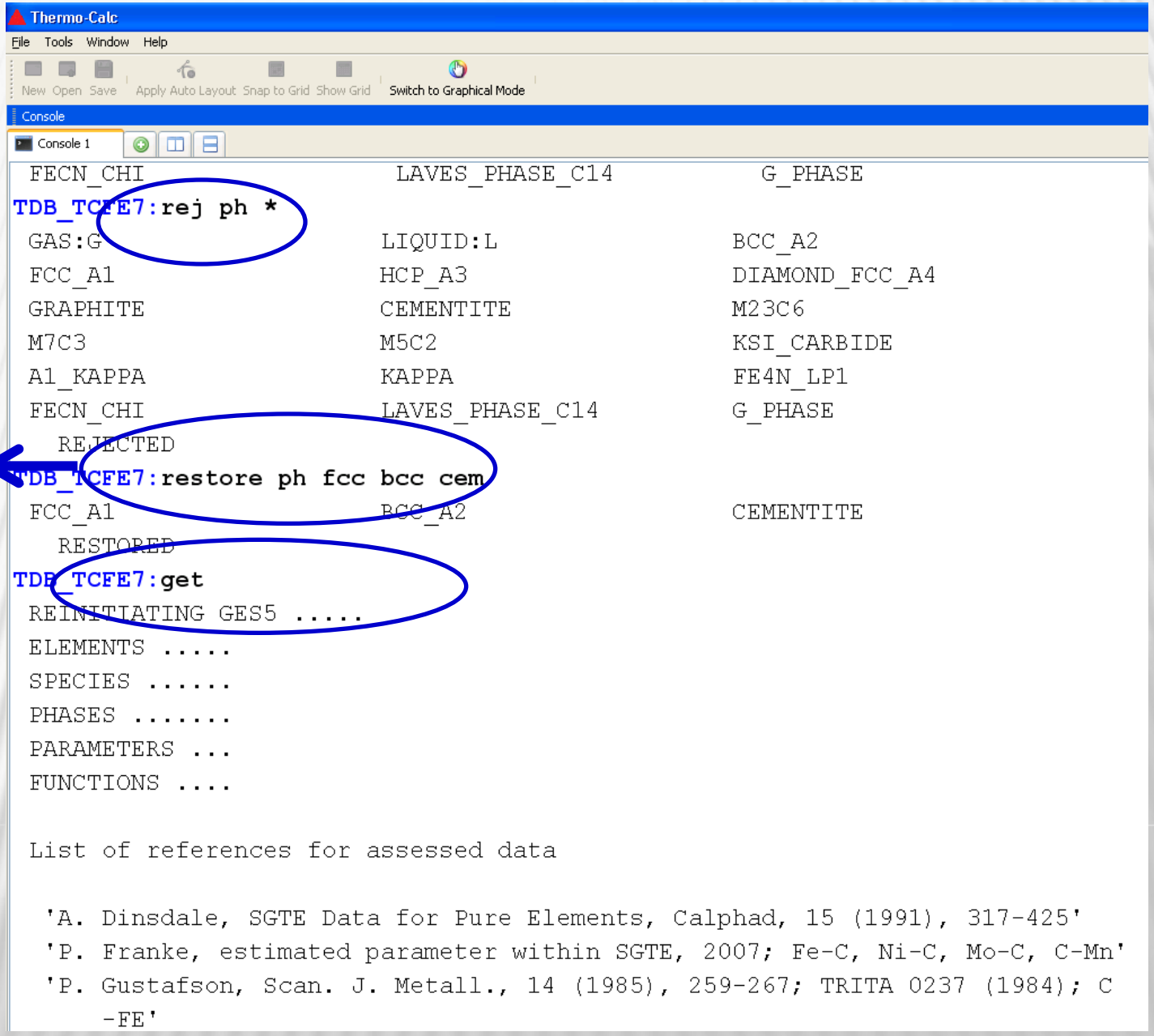

Condiciones: P,T, composiciones....

ISOPLETH

```
TDB_TCFE7:go p-3

 POLY version 3.32
POLY_3:s-c p=1e5 n=1 t=1200 x(c)=0.03 x(mn)=0.1
POLY_3:l-c
 P=1E5, N=1, T=1200, X(C)=3E-2, X(MN)=0.1
 DEGREES OF FREEDOM 0
POLY_3:c-e
 Global equilibrium calculation turned off, you can turn it on with
 ADVANCED_OPTIONS GLOBAL_MINIMIZATION Y,,,,,,,,
    16 ITS,  CPU TIME USED   0 SECONDS
POLY_3:s-a-v 1 x(c)
Min value /0/:
Max value /1/:
Increment /.025/:
POLY_3:s-a-v 2 t
Min value /0/:400
Max value /1/:1200
Increment /20/:
POLY_3:save
```

2.- CÁLCULO DE DIAGRAMAS DE FASE: ISOPLETH E ISOTHERM

```
POLY_3:map
 Version S mapping is selec

POLY_3:post

   POLY-3 POSTPROCESSOR VERS


 Setting automatic diagram

POST:plot
```

```
POST:s-s-s x n 0 0.1
POST:s-s-s y n 600 1000
POST:s-lab e
POST:plot
```

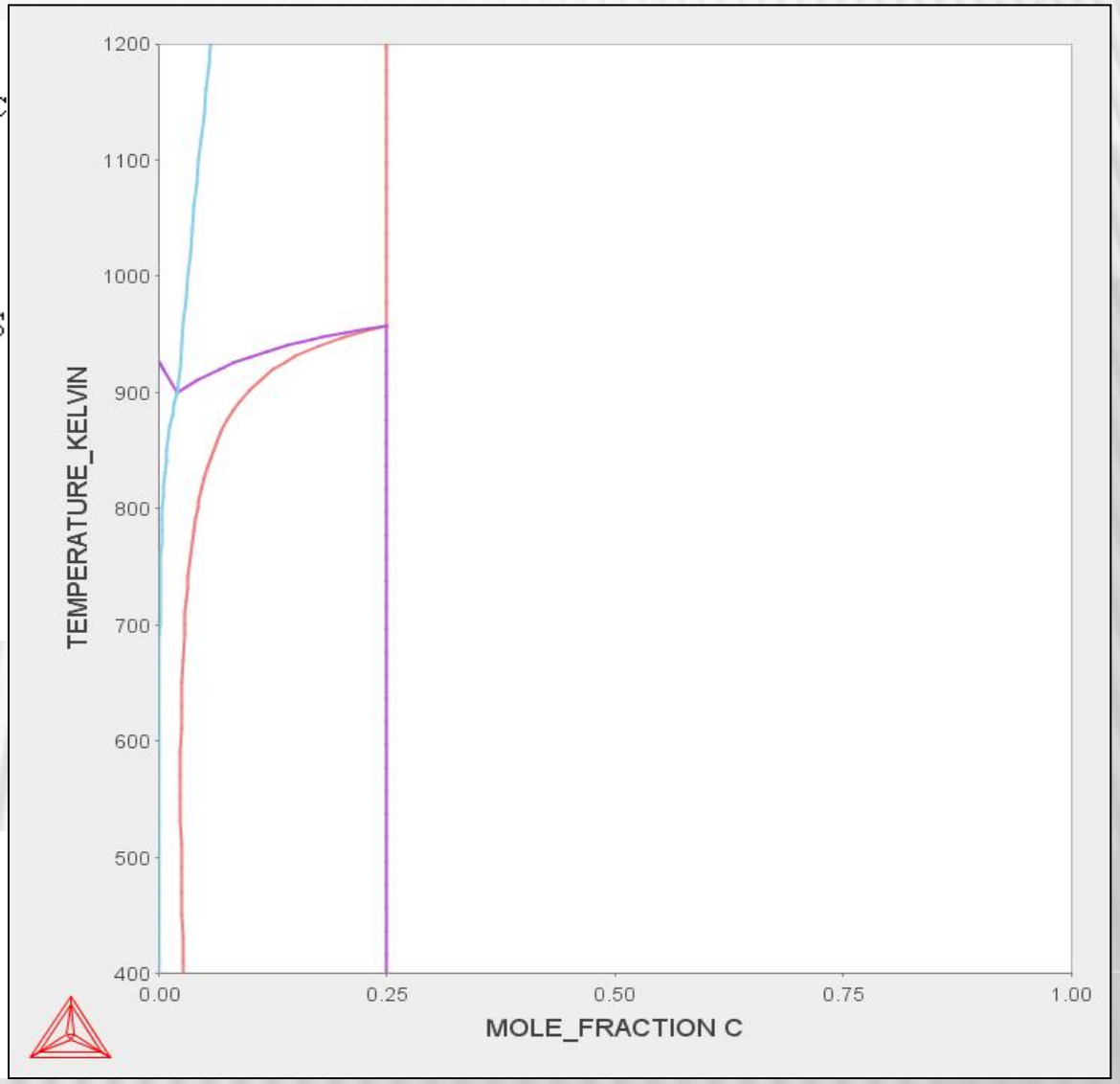

2.- CÁLCULO DE DIAGRAMAS DE FASE: ISOPLETH E ISOTHERM

SELECCIÓN DE TEMPERATURA PARA LOS TRATAMIENTOS ISOTÉRMICOS

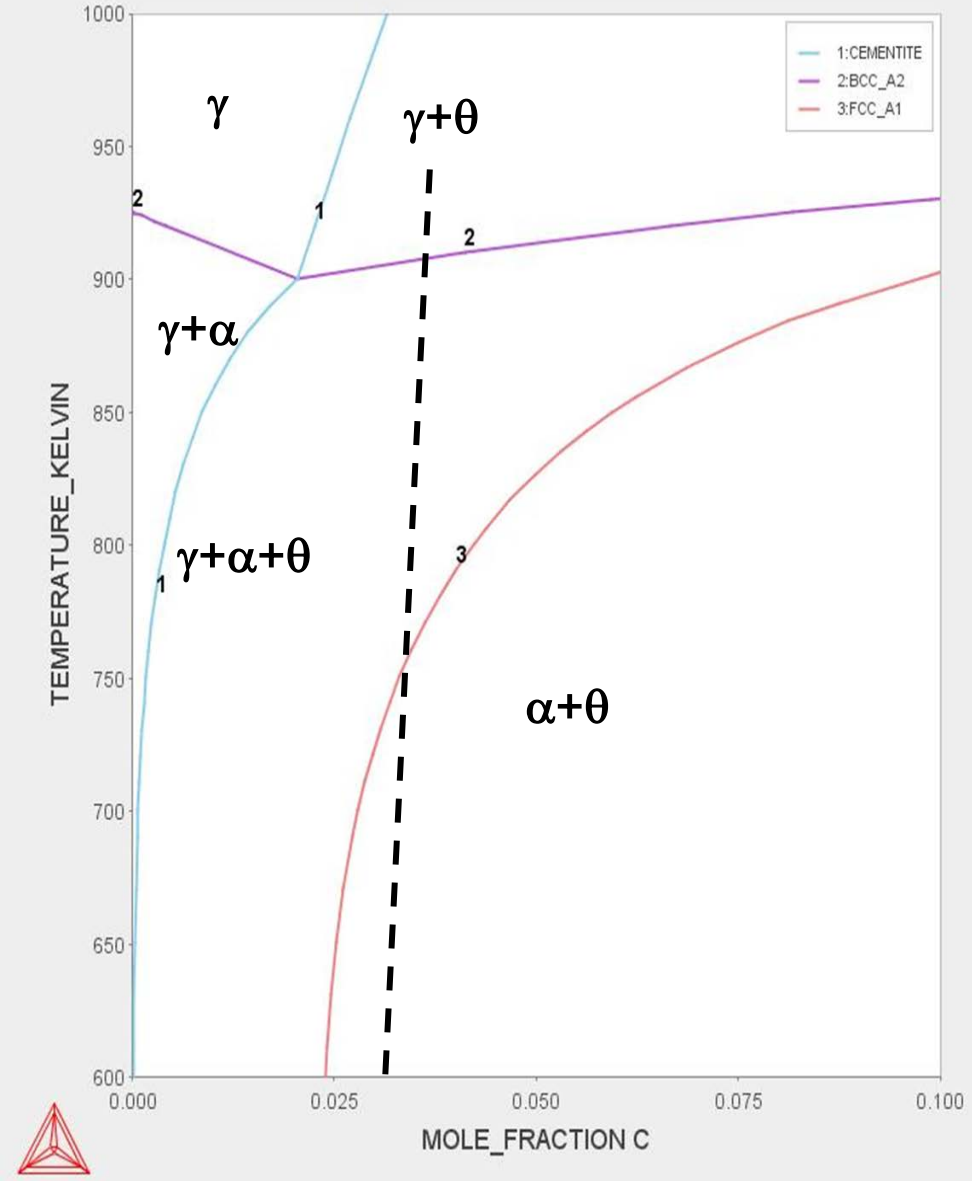

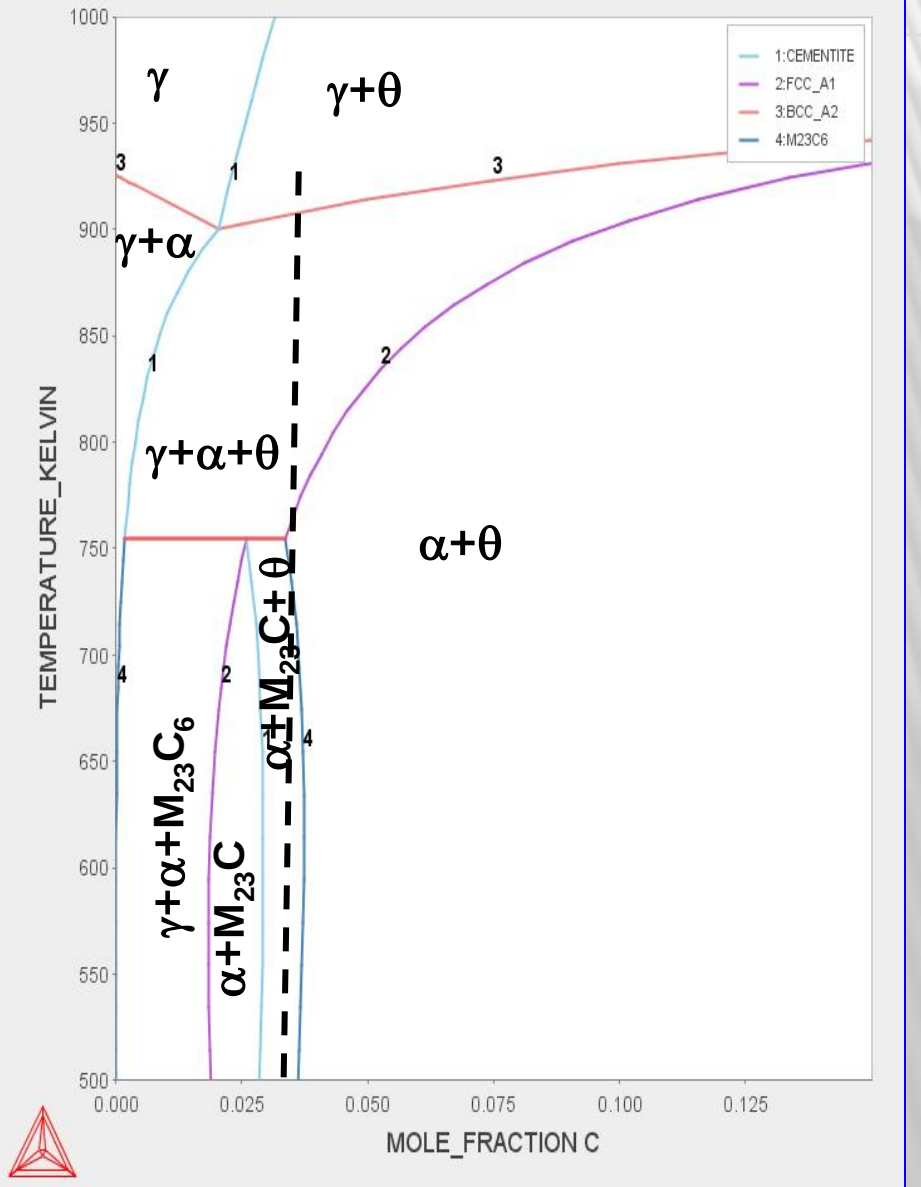

2.- CÁLCULO DE DIAGRAMAS DE FASE: ISOPLETH E ISOTHERM

```
 POLY version  3.32
POLY_3:s-c t=873 n=1 p=1e5 x(c)=0.03 x(mn)=0.1
POLY_3:l-c
 T=873, N=1, P=1E5, X(C)=3E-2, X(MN)=0.1
 DEGREES OF FREEDOM 0
POLY_3:c-e
 Global equilibrium calculation turned off, you can turn it on with
 ADVANCED_OPTIONS GLOBAL_MINIMIZATION Y,,,,,,,,
    19 ITS,  CPU TIME USED    0 SECONDS
POLY_3:s-a-v 1 x(c) 0 1
Increment /.025/:
POLY_3:s-a-v 2 x(mn) 0 1
Increment /.025/:
POLY_3:map
```

ISOTHERM

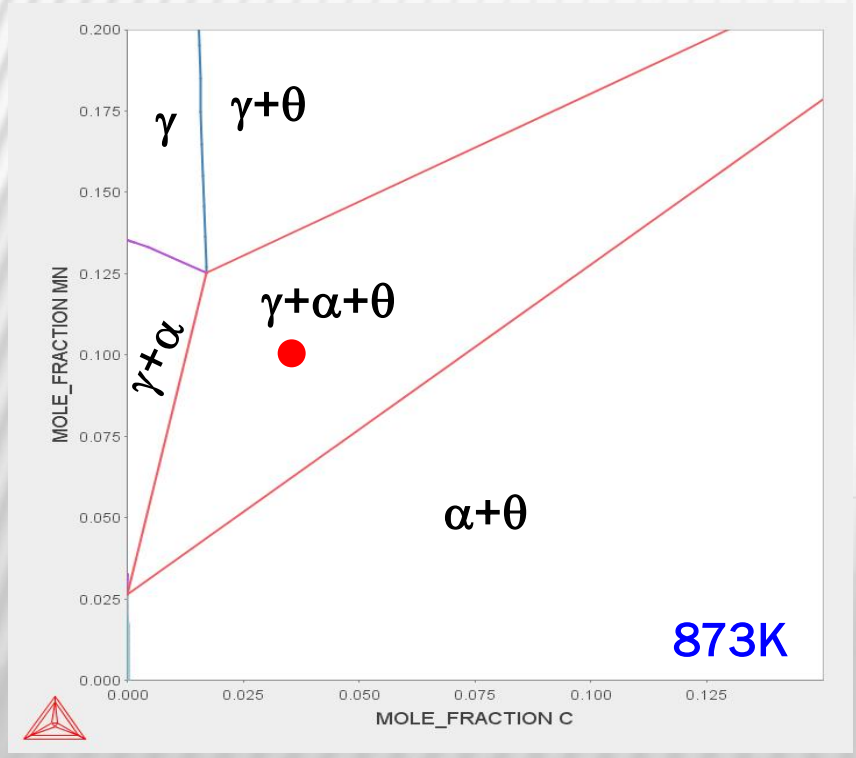

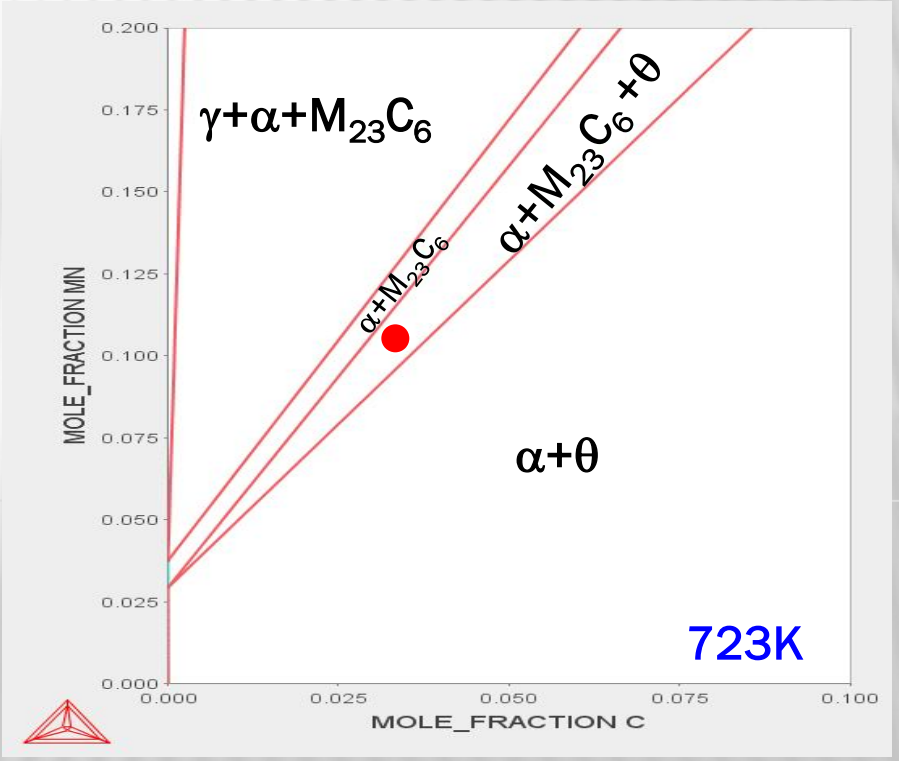

EXTRAPOLACIÓN DE HULTGREN: EXTRAPOLACIÓN DE LAS LÍNEAS

γ/γ+α

γ/γ+ θ

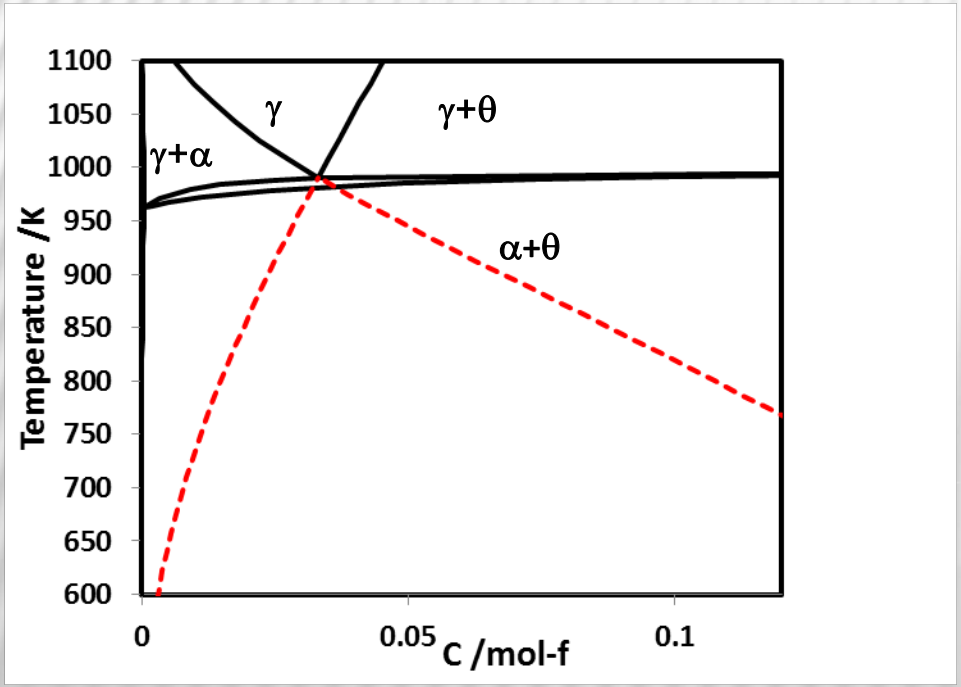

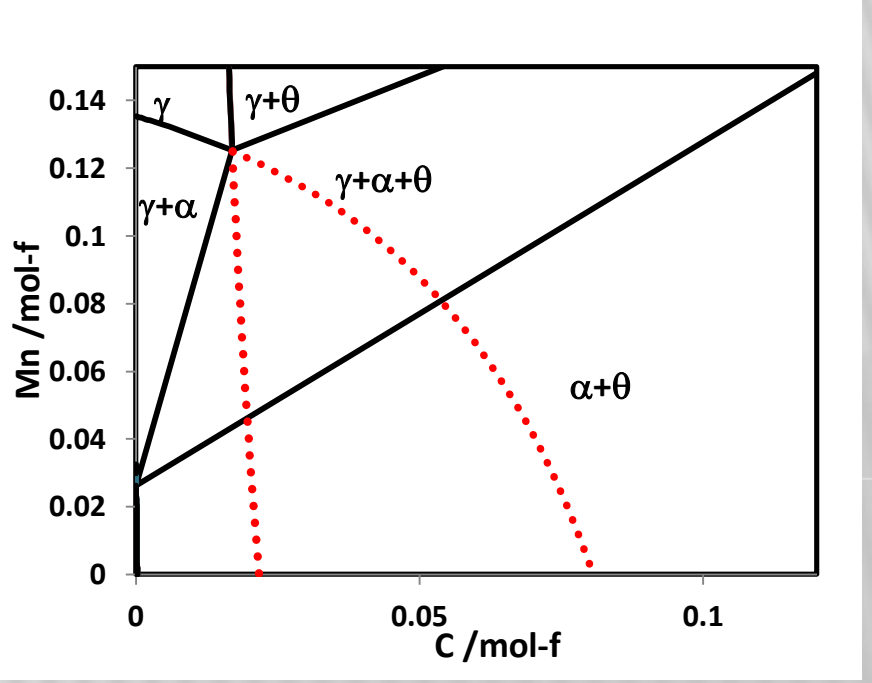

3.- EXTRAPOLACIÓN DE LAS LÍNEAS γ/γ+α γ/γ+ θ

Thermo-Calc

File Tools Window Help

New Open Save | Apply Auto Layout Snap to Grid Show Grid | Switch to Graphical Mode

Console

Console 1

```
SYS:go d
 THERMODYNAMIC DATABASE module
 Current database: TCS Steels/Fe-Alloys Database v7.0
 VA  DEFINED
 L12_FCC              B2_BCC              B2_VACANCY
 HIGH_SIGMA           DICTRA_FCC_A1  REJECTED
TDB_TCFE7:def-sys fe c mn
 FE                   C                   MN
   DEFINED
TDB_TCFE7:rej ph *
TDB_TCFE7:restore ph fcc bcc
TDB_TCFE7:get
TDB_TCFE7:go p-3
POLY version  3.32
POLY_3:s-c t=873 n=1 p=1e5 x(mn)=0.1 x(c)=0.03
POLY_3:l-c
 T=873, N=1, P=1E5 ,X(MN)=1E-1, X(C)=0.03

 DEGREES OF FREEDOM 0
POLY_3:c-e
POLY_3:s-a-v 1 x(c) 0 1
Increment /.025/:
POLY_3:s-a-v 2 x(mn) 0 1
POLY_3:map
POLY_3:post
POST:s-s-s x n  0 0.15
POST:s-s-s y n  0 0.15
POST:pl
```

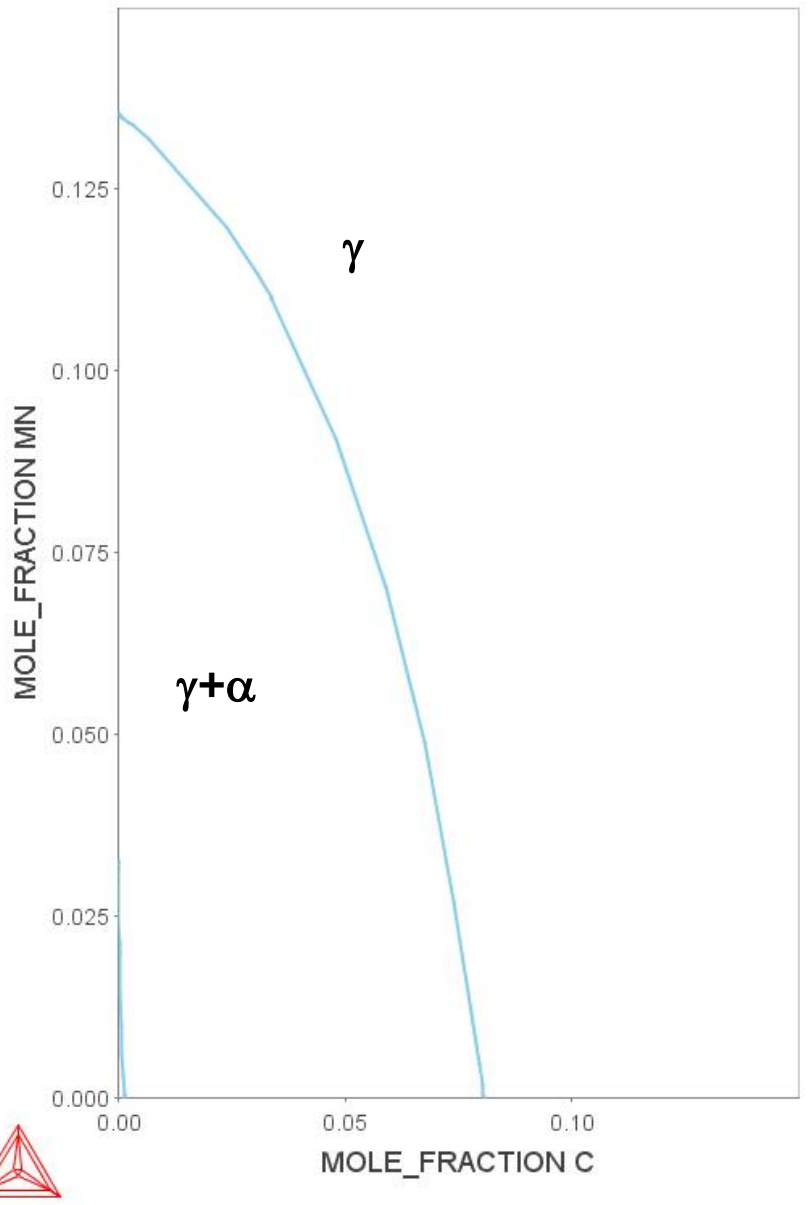

Superposición de las líneas γ/γ+α y γ/γ+ θ en el diagrama de fases

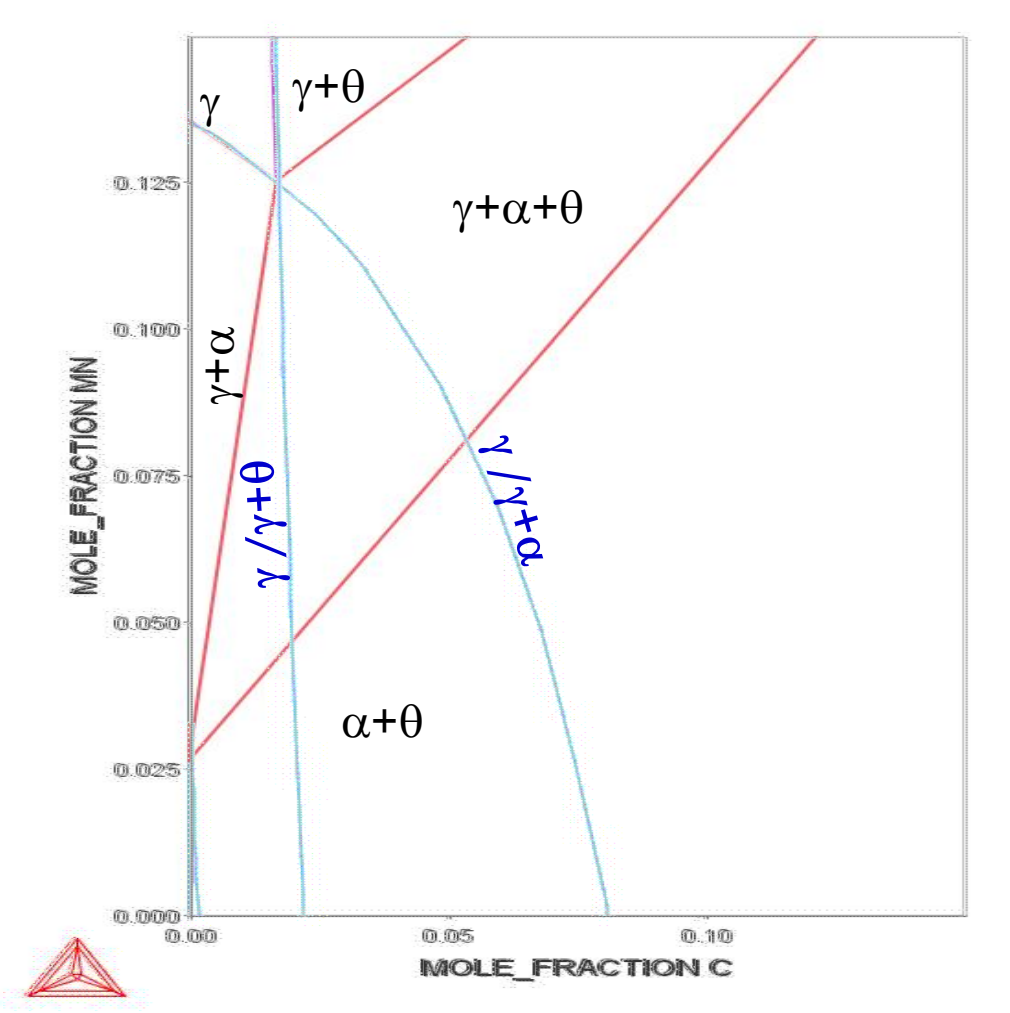

LÍNEAS DE PARTICIÓN-NO PARTICIÓN

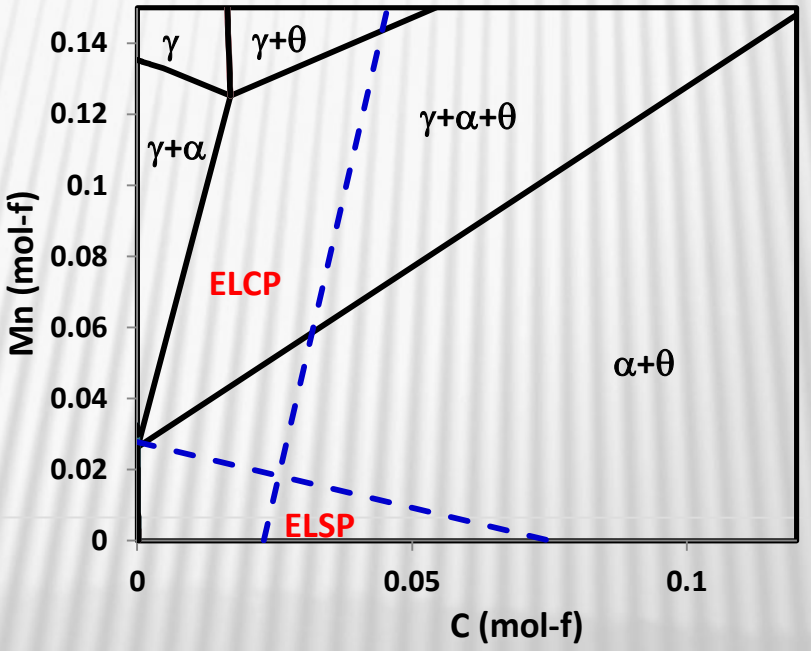

4.- LÍNEAS DE PARTICIÓN-NO PARTICIÓN

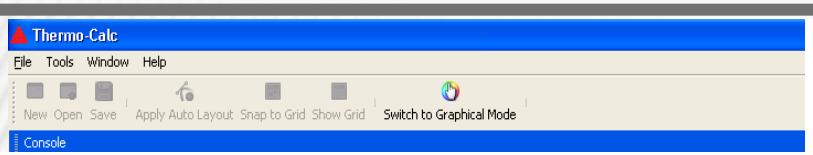

SYS:go d

@SÓLO TENDREMOS EN CUENTA LA FASE AUSTENITA y FERRITA!, todas las demás fases las suspenderemos.

HIGH_SIGMA DICTRA_FCC_A1 REJECTED
TDB_TCFE7:def-sys fe c mn
FE C MN
DEFINED
TDB_TCFE7:rej ph *
TDB_TCFE7:restore ph fcc bcc
TDB_TCFE7:get
TDB_TCFE7:go p-3
POLY version 3.32
POLY_3:s-c t=873 n=1 p=1e5 x(mn)=0.1 x(c)=0.03
POLY_3:l-c
T=873, N=1, P=1E5 ,X(MN)=1E-1, ACR(C)=0.055

DEGREES OF FREEDOM 0
POLY_3:c-e
POLY_3:s-a-v 1 x(c) 0 1
Increment /.025/:
POLY_3:s-a-v 2 x(mn) 0 1
POLY_3:map
POLY_3:post
POLY_3:s-t-s 1
POST:s-s-s x n 0 0.1
POST:s-s-s y n 0.15
POST:pl

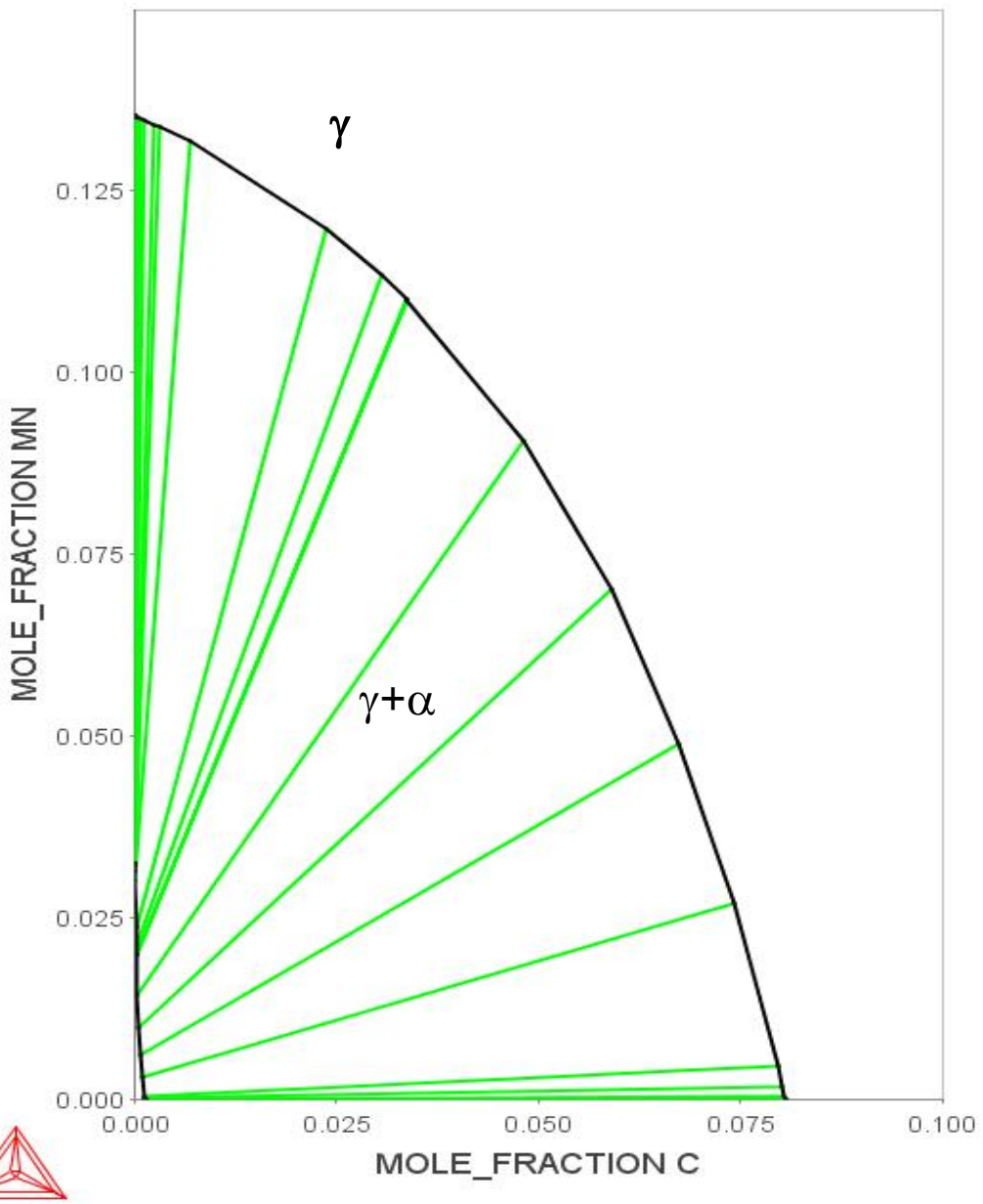

4.- LÍNEAS DE PARTICIÓN-NO PARTICIÓN

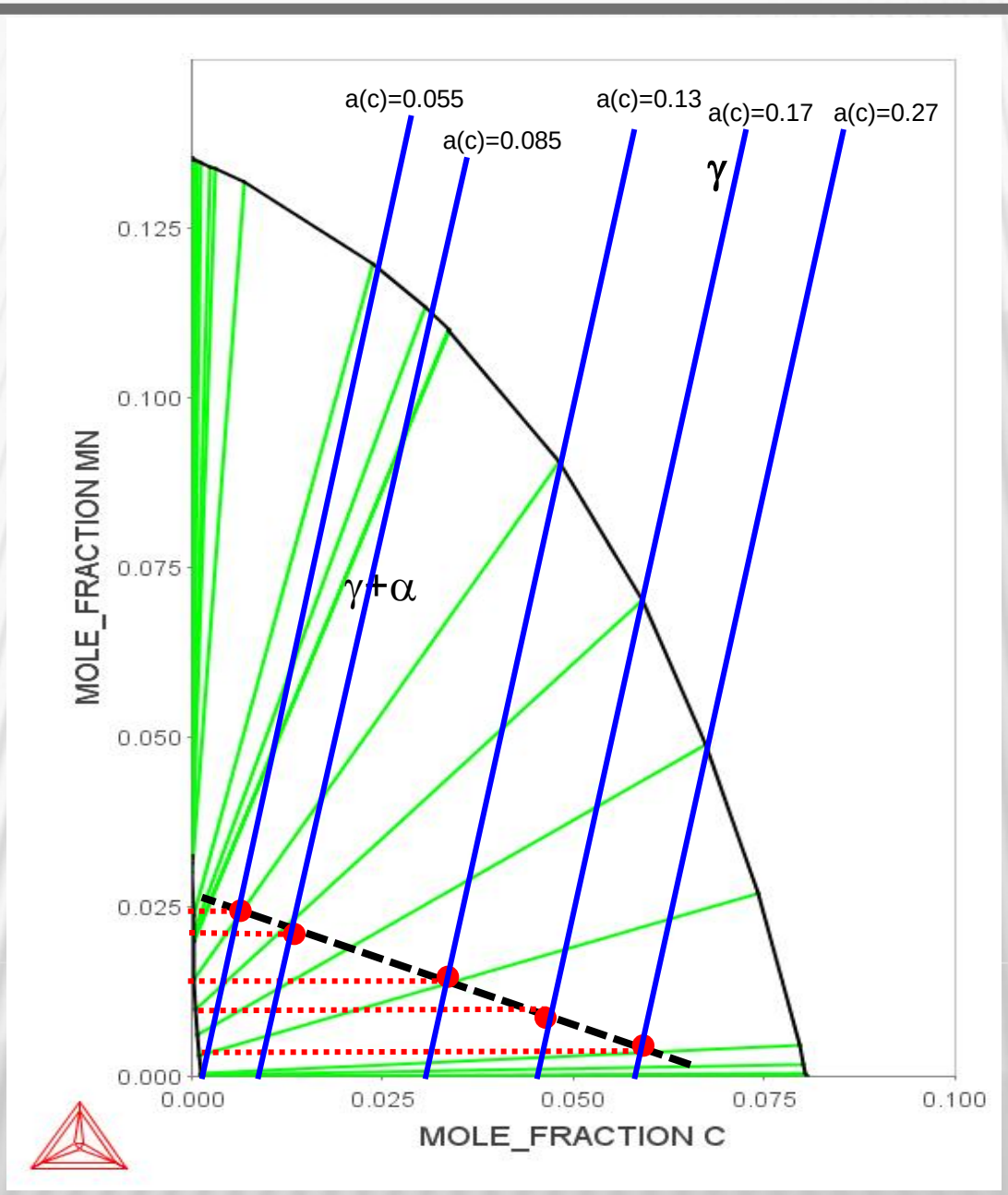

4.- LÍNEAS DE PARTICIÓN-NO PARTICIÓN

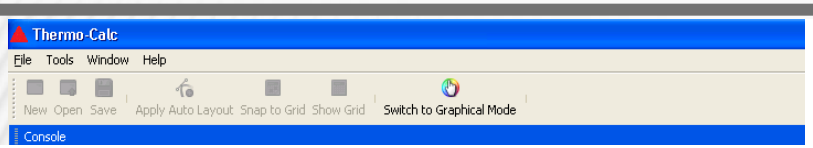

SYS:go d

@Para calcular las líneas de isoactividad
SÓLO TENDREMOS EN CUENTA LA FASE AUSTENITA!,
todas las demás fases las suspenderemos.

TDB_TCFE7:def-sys fe c mn
FE C MN
DEFINED
TDB_TCFE7:rej ph *
TDB_TCFE7:restore ph fcc
TDB_TCFE7:get
TDB_TCFE7:go p-3
POLY version 3.32
POLY_3:s-c t=873 n=1 p=1e5 x(mn)=0.1 acr(c)=0.055
POLY_3:l-c
T=873, N=1, P=1E5 ,X(MN)=1E-1, ACR(C)=0.055

DEGREES OF FREEDOM 0
POLY_3:c-e
POLY_3:s-a-v 1 x(mn) 0 1
Increment /.025/:
POLY_3:step
POLY_3:post
POLY_3:s-d-a x x(c)
POLY_3:s-d-a y x(mn)
POST:s-s-s x n 0 0.1
POST:s-s-s y n 0.15
POST:pl

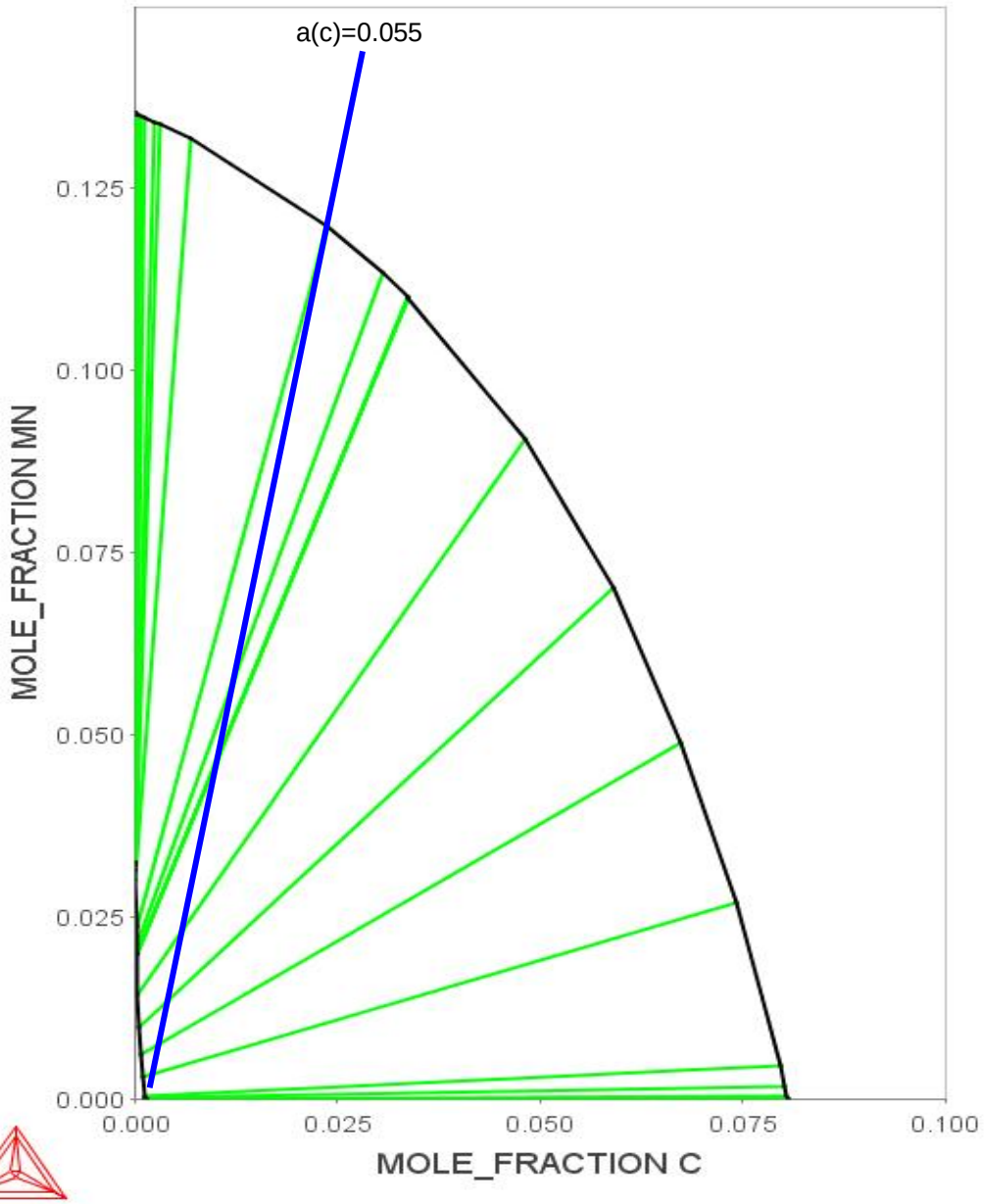

4.- LÍNEAS DE PARTICIÓN-NO PARTICIÓN

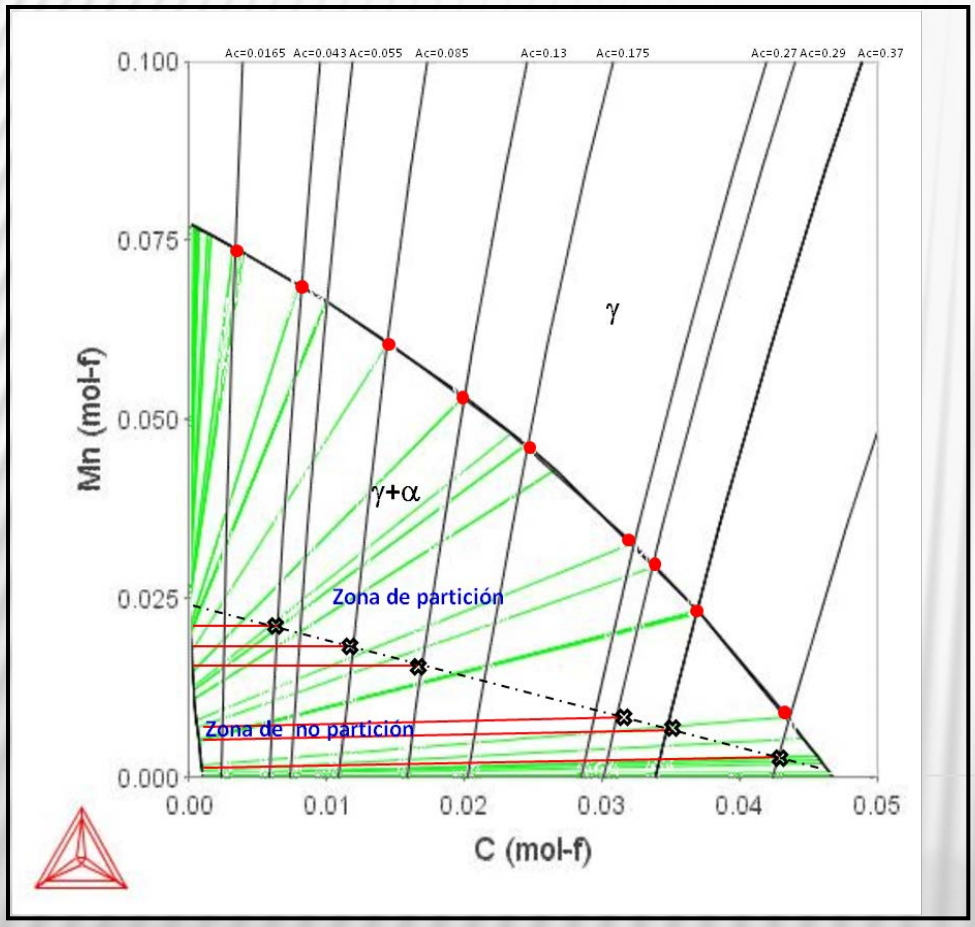

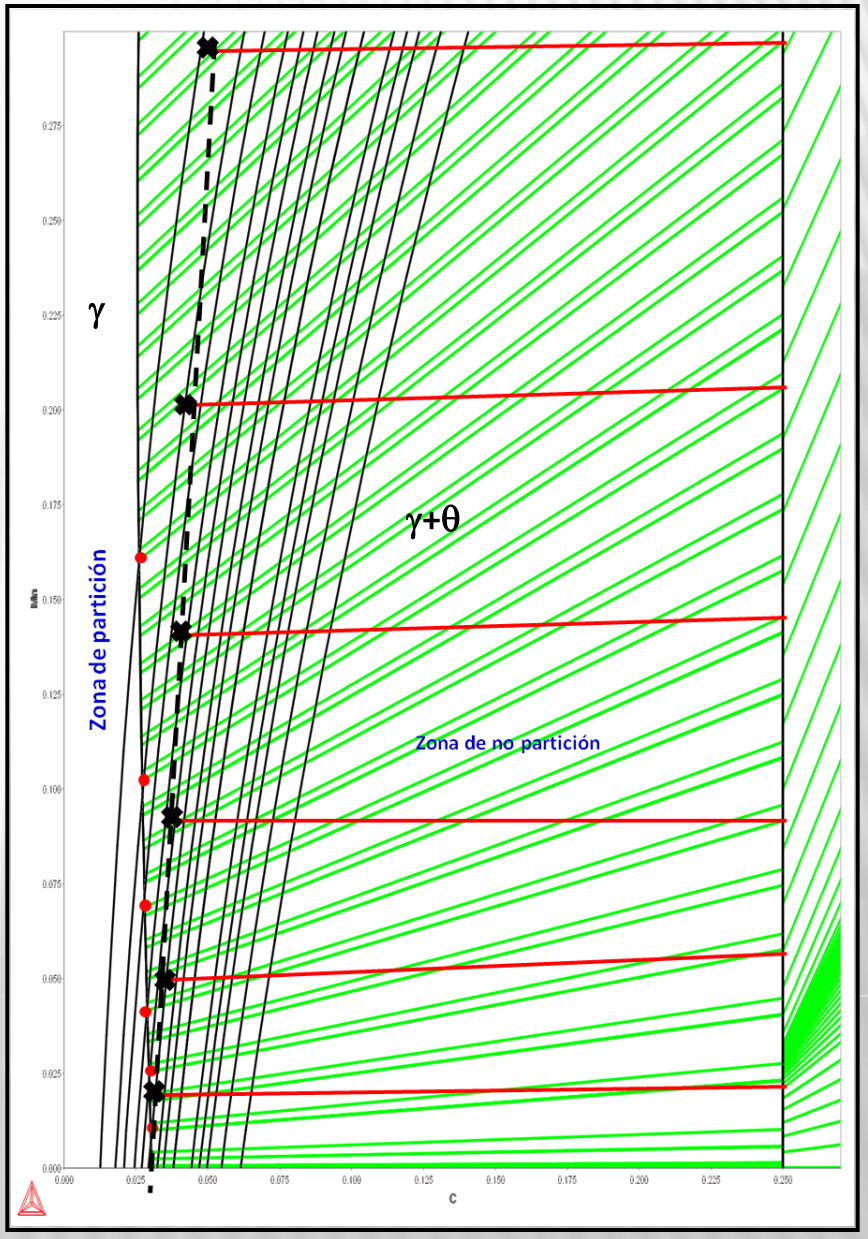

Crecimiento de perlita con partición (ELCP) y sin partición (ELSP) de Mn.

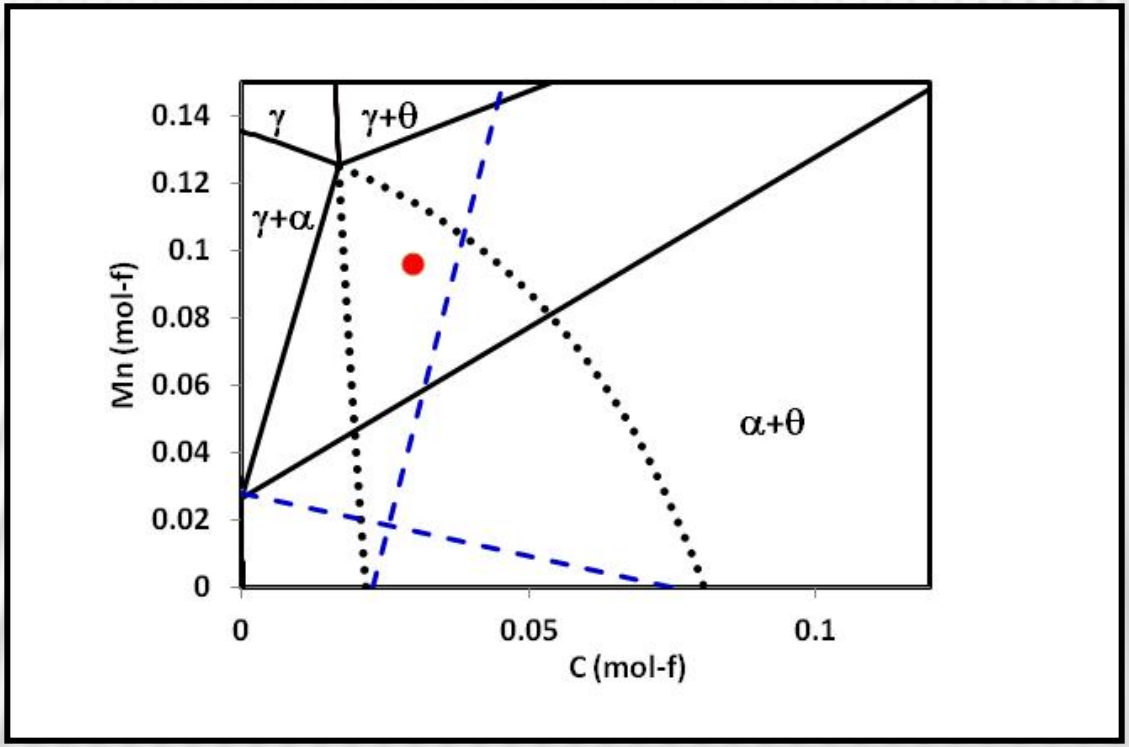

COMPOSICIÓN DE LAS INTERCARAS

$\gamma/\gamma+\alpha$

$\gamma/\gamma+\theta$

EQUILIBRIO LOCAL Y EQUILIBRIO

- PERLITA CONSTANTE
- PERLITA DIVERGENTE

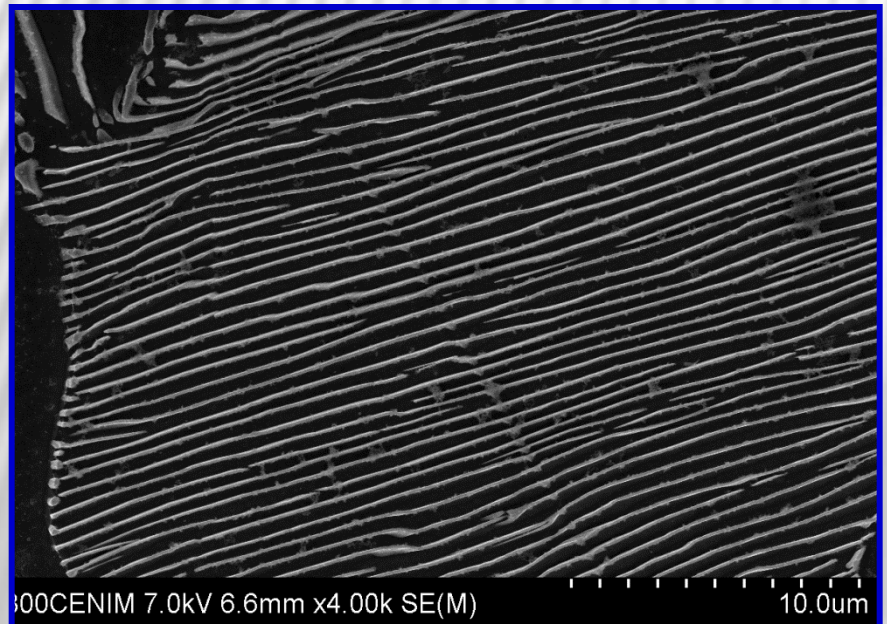

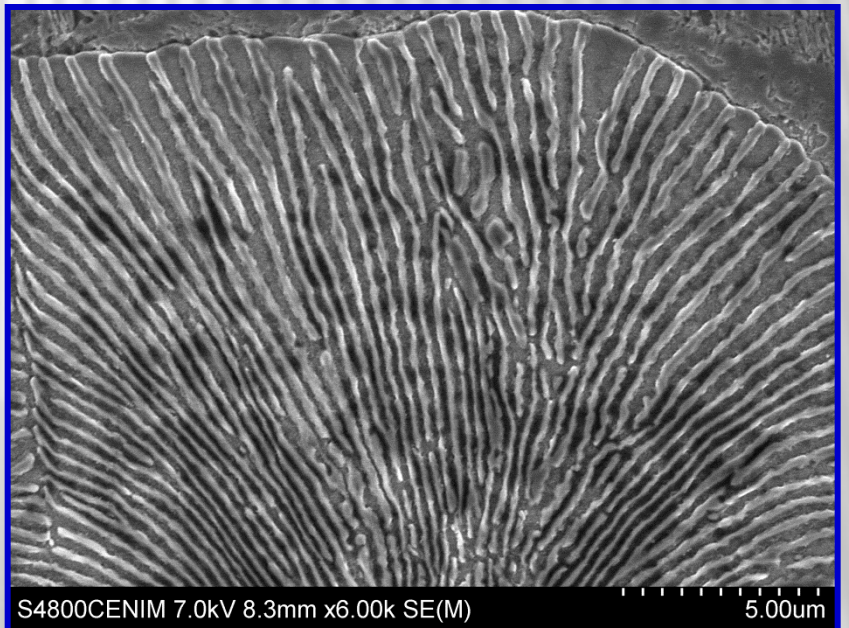

5.- COMPOSICIÓN DE LAS FASES

EL PERLITA CONSTANTE

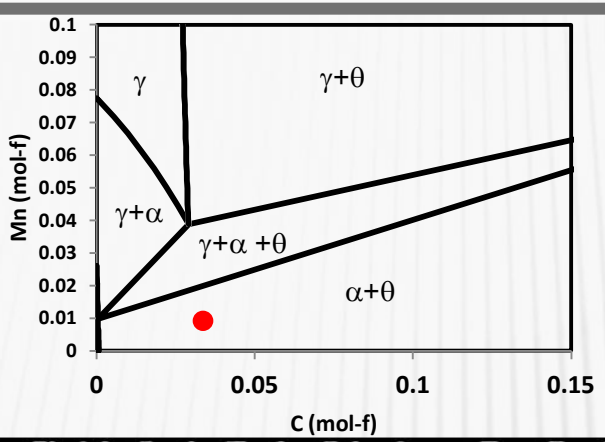

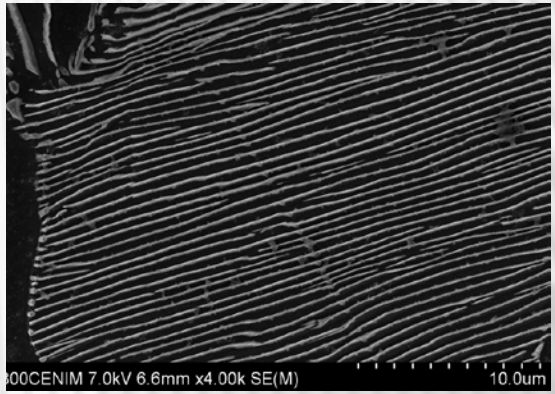

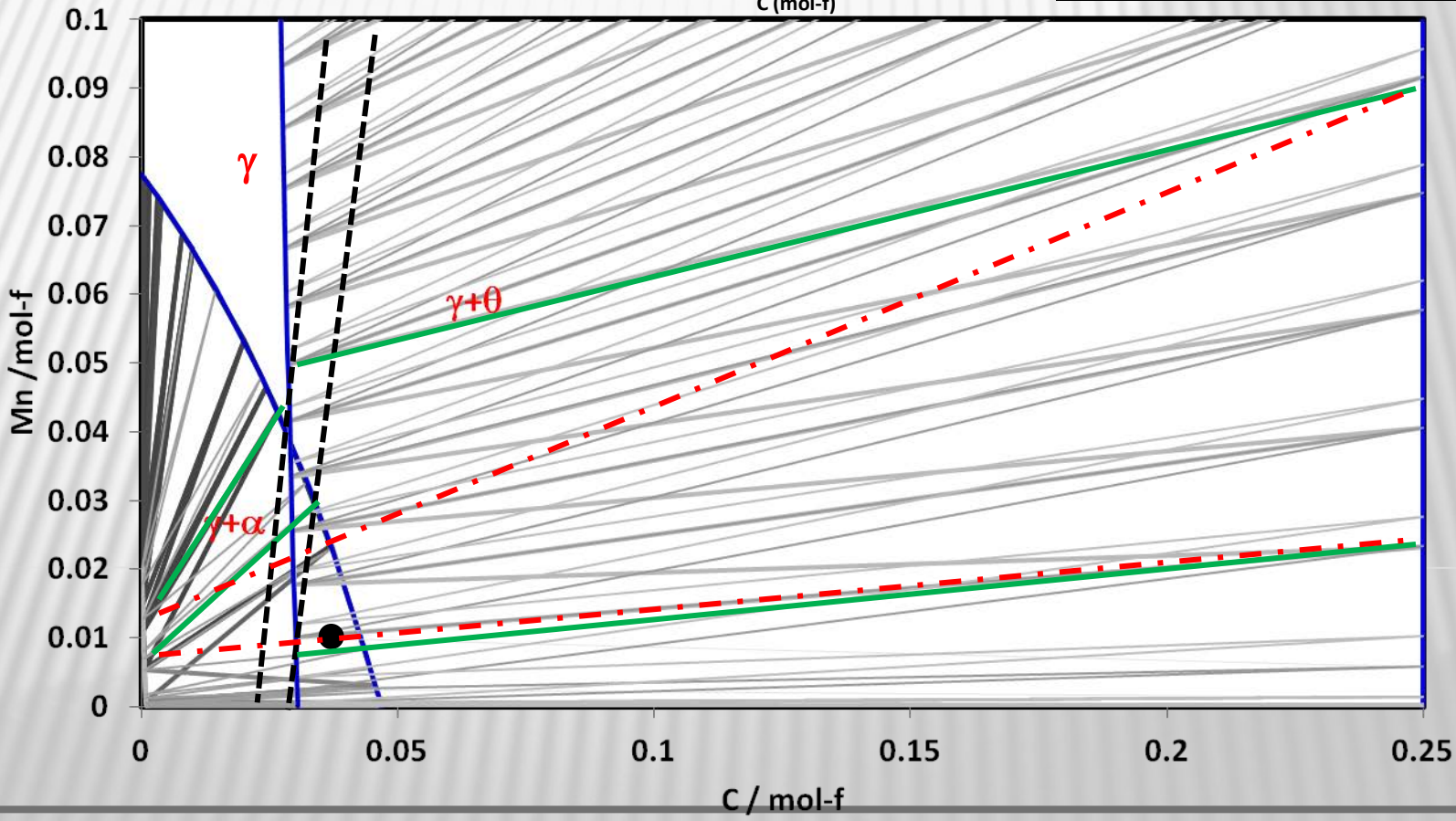

5.- COMPOSICIÓN DE LAS FASES

EQ PERLITA CONSTANTE

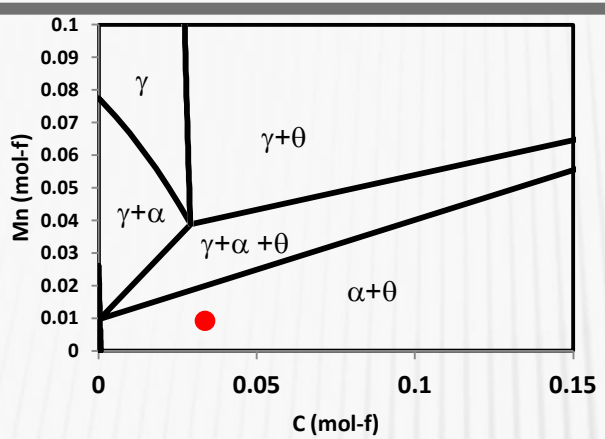

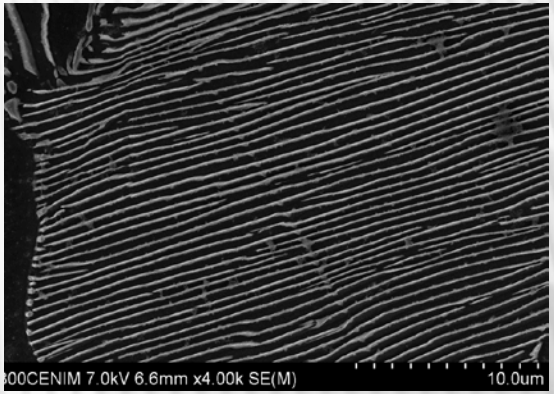

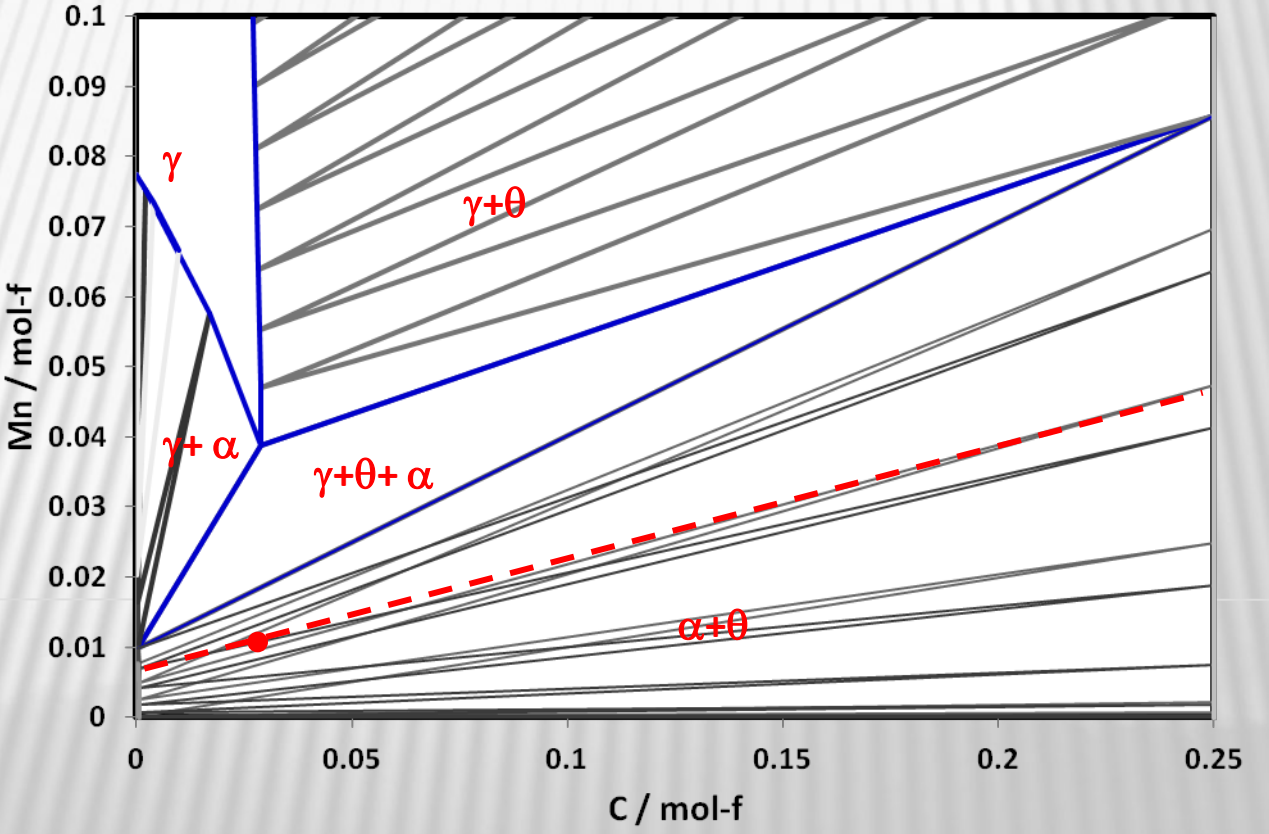

5.- COMPOSICIÓN DE LAS FASES

EL PERLITA DIVERGENTE

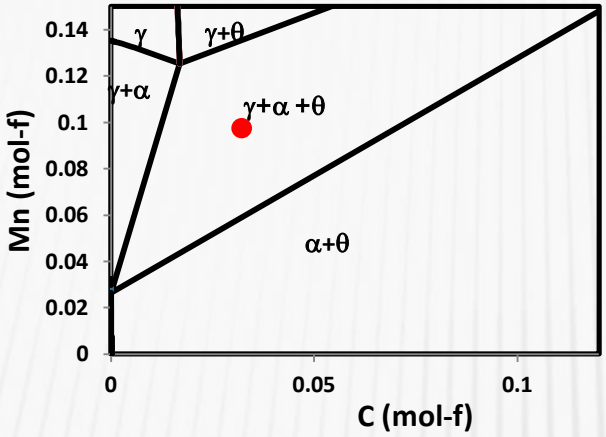

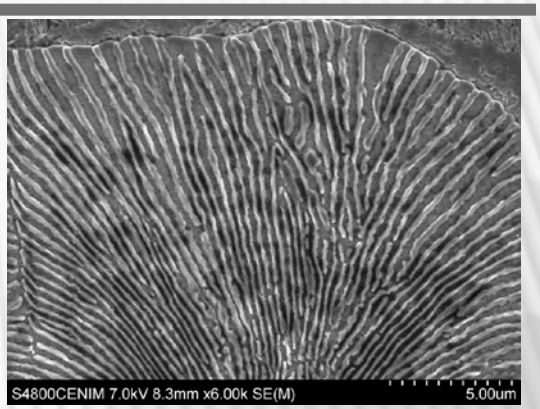

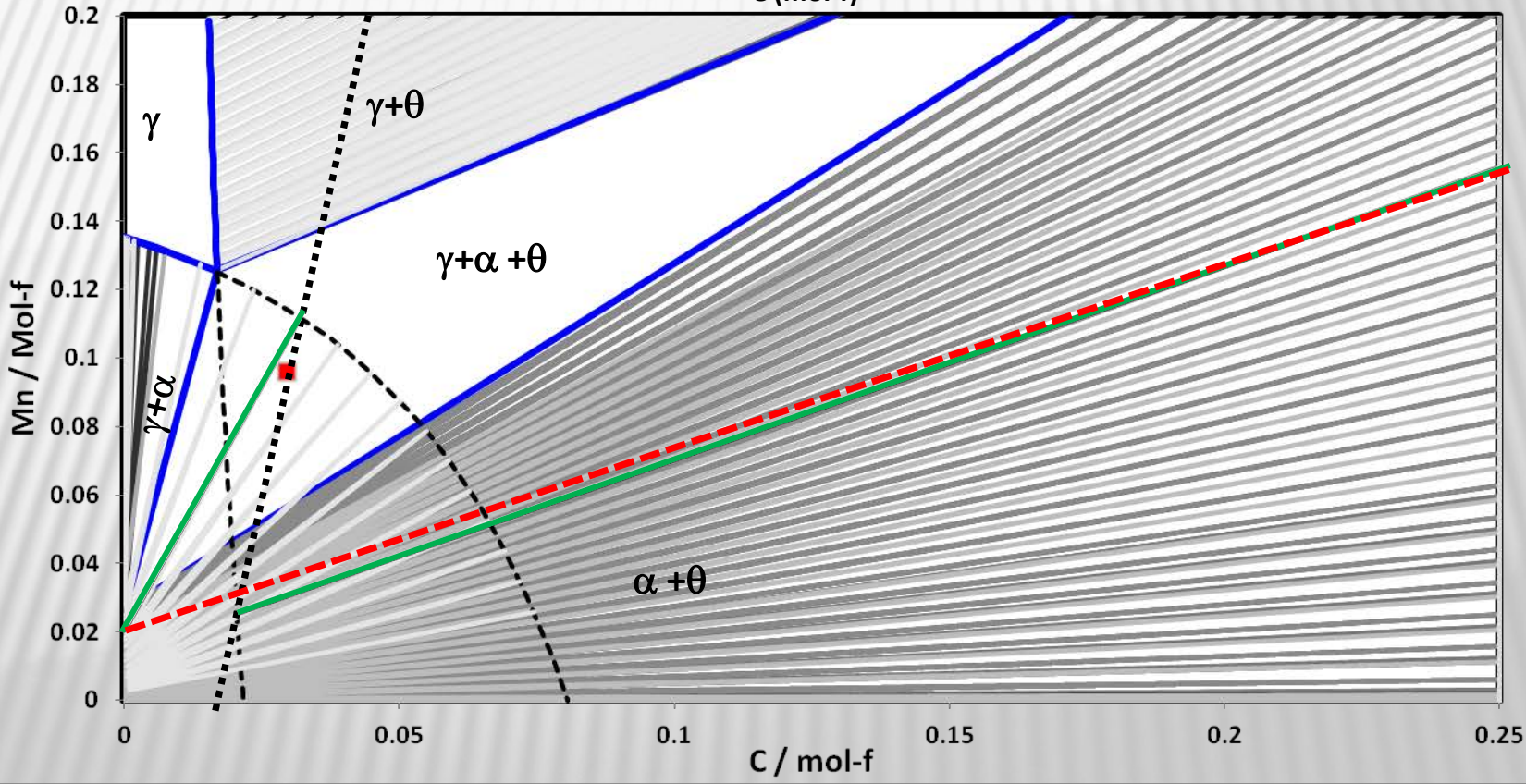

5.- COMPOSICIÓN DE LAS FASES

EQ PERLITA DIVERGENTE

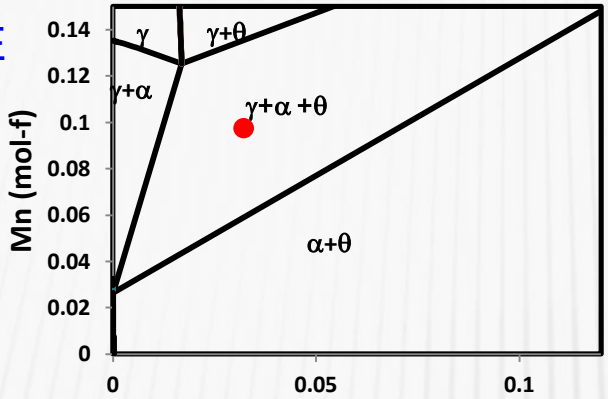

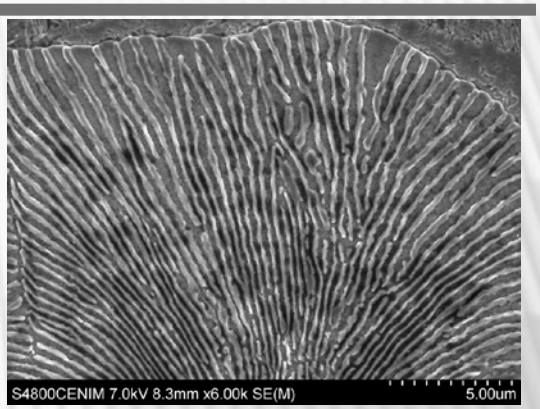

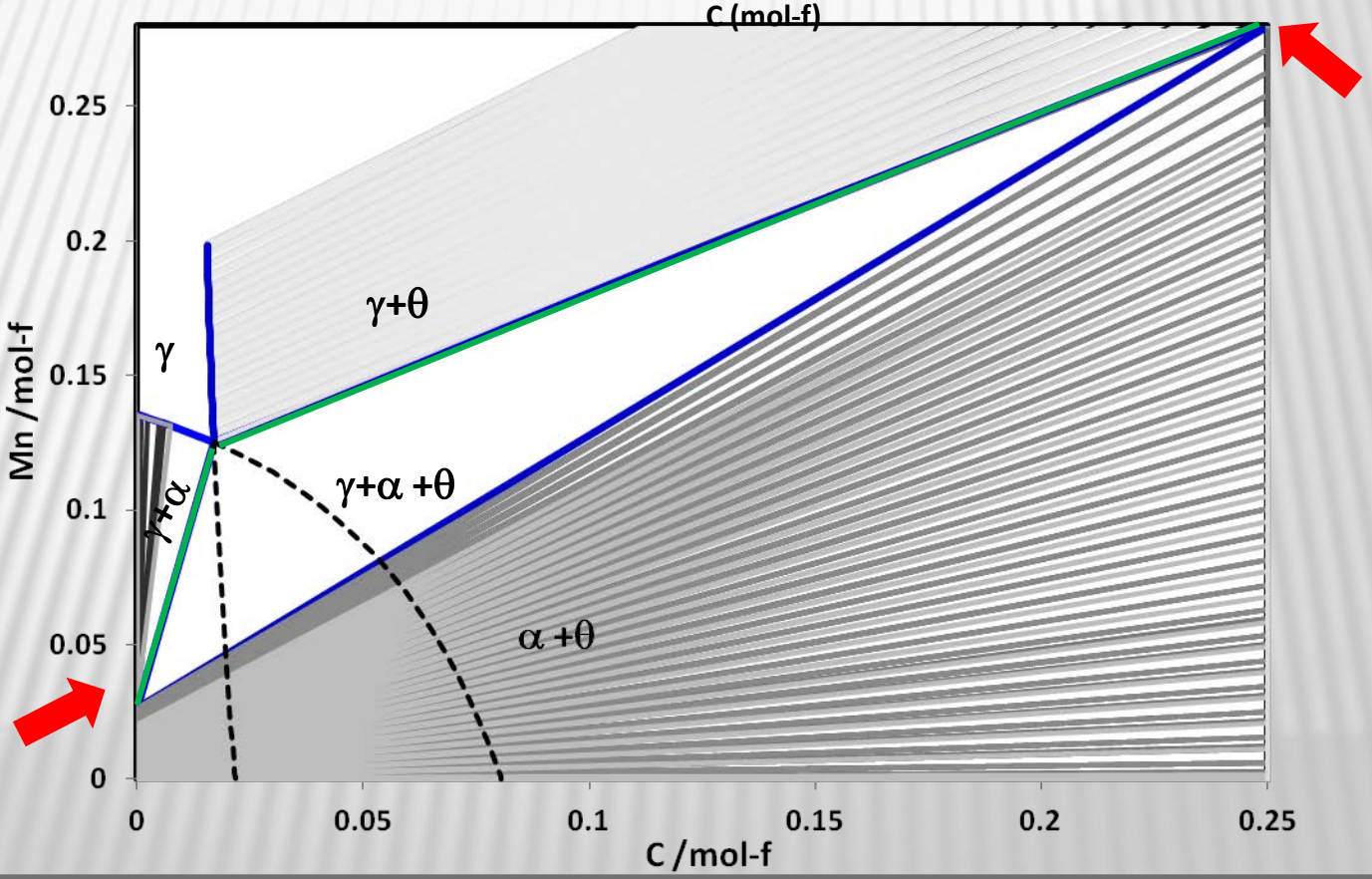

¡¡¡GRACIAS POR SU ATENCIÓN !!!